COLLECTIVE BEHAVIOR

Self-reconfigurable multilegged robot swarms collectively accomplish challenging terradynamic tasks

Yasemin Ozkan-Aydin[1,2]* and Daniel I. Goldman[2]

Swarms of ground-based robots are presently limited to relatively simple environments, which we attribute in part to the lack of locomotor capabilities needed to traverse complex terrain. To advance the field of terradynamically capable swarming robotics, inspired by the capabilities of multilegged organisms, we hypothesize that legged robots consisting of reversibly chainable modular units with appropriate passive perturbation management mechanisms can perform diverse tasks in variable terrain without complex control and sensing. Here, we report a reconfigurable swarm of identical low-cost quadruped robots (with directionally flexible legs and tail) that can be linked on demand and autonomously. When tasks become terradynamically challenging for individuals to perform alone, the individuals suffer performance degradation. A systematic study of performance of linked units leads to new discoveries of the emergent obstacle navigation capabilities of multilegged robots. We also demonstrate the swarm capabilities through multirobot object transport. In summary, we argue that improvement capabilities of terrestrial swarms of robots can be achieved via the judicious interaction of relatively simple units.

INTRODUCTION

In a variety of environments, animals such as insects [honeybees (1), ants (2–4), termites (5, 6), etc.], fishes (7), and birds (8) can self-organize and create structures to solve problems that are difficult or impossible for single individuals to accomplish. Emergent collective behaviors can arise from relatively simple rules followed by individuals through local and limited communication between agents and interactions with the environment (8). Inspired by the capabilities of biological swarms, researchers have developed aerial, underwater, and ground-based robotic swarming systems that can robustly navigate in the real world (9), performing tasks such as mapping, tracking, inspection, and transportation (10). A key enabler of swarming task completion is the ability of individuals to locomote in the environment. Compared with unstructured and dynamic terrestrial environments, air and water are relatively homogeneous and predictable, which simplifies the design of swarm algorithms in the presence of proper robotic systems. With the development of commercially available robust automated aerial and underwater vehicles, researchers are now able to move the robots out of laboratories and successfully implement swarm behaviors in real-world aerial/aquatic environments (11, 12).

Terrestrial swarms face unique challenges compared with their aerial and aquatic counterparts. First, relative to the robust locomotor capabilities of individuals in fluid-based swarms, individuals in terrestrial swarms are still limited to relatively simple environments, such as smooth factory floors or pavement. This is largely because such individuals typically consist of vehicles having wheels/tracks, which are effective in two-dimensional (2D) environments (13) but face challenges navigating over obstacles, such as bumpy terrain or areas with low friction (14–16). Some of these challenges have been addressed in the decades of research on locomotion of individual robots in complex terrestrial terrain. These studies have led to discoveries of important "terradynamic" interactions (17), control of which has improved locomotor performance (18–21). One way that

effective terradynamic interactions can be generated is through the use of appendages, such as limbs and tails: Increasing the understanding of principles of limb use in robots (22–24) [taking insight from living systems (25)] offers effective body support and enable rapid maneuverability (26, 27), facilitating obstacle crossing (28, 29) and climbing (30, 31). However, although major advances have occurred in legged robots (32–34), the most robust devices are thought to require high numbers of degrees of freedom (DoFs), complex control, and gait planning to operate robustly (35–38). The selection of a suitable gait requires an appreciable modeling and control effort for improving mobility with legs in unstructured environments (39–42). This makes such complex devices unsuitable for scaling up to many robots in a swarm, but recent work on the use of passive mechanics and mechanisms (43, 44) has made it possible to create swarms of legged robots that are robust and cost efficient.

Terrestrial swarms also have member interaction features that differ from aquatic and aerial swarms and can offer opportunities: Whereas individuals in fluid-based biological and robotic swarms tend to avoid direct contact and collisions, in terrestrial environments, swarms can gain advantages through physical contact between individuals, as in biological systems. Inspired by the collective behaviors of social terrestrial insects (3, 5, 45, 46), many researchers have studied self-assembling or reconfigurable modular swarm robots in which individual units can connect to form robotic structures with different shapes and functions (47–52). However, in most studies of self-reconfigurable robotic systems, the units of a swarm either have limited motive abilities and require some level of human intervention to form desired configurations (53–56) or the assembly process completely relies on stochastic interaction between individuals (57–60). Although these approaches are potentially advantageous because they produce low-cost, scalable, and robust morphologies, they often underestimate real-world locomotion problems by focusing on the interaction between individuals, rather than the environment.

Previous research showed that the physical connection between swarms of robots could enable them to overcome obstacles in moderately rough terrain (50, 61, 62). Depending on tasks and environment, such robots connect to each other and dynamically change shape to handle real-world problems without centralized planning and control (61, 63). This approach improves the mobility of a terrestrial

[1]Department of Electrical Engineering, University of Notre Dame, Notre Dame, IN 46556, USA. [2]School of Physics, Georgia Institute of Technology, Atlanta, GA 30332, USA.
*Corresponding author. Email: yozkanay@nd.edu

collective system and provides strong robustness to failures by exploiting the physical connections between individuals. However, their results were limited by the fact that the wheeled/track robots could not overcome complex terrain accessible to legged robots.

Here, we propose a path toward a terradynamically capable decentralized legged swarm that can reconfigure to solve mobility challenges that individual legged robots encounter (Movie 1). Taking the minimalist robotic approach, which provides powerful platforms for testing biological hypotheses about mechanical design and movement control strategies (64, 65), we investigate legged swarm dynamics and improve the motion agility in a variety of environments (including rough terrain, hard ground, obstacle climbing, etc.). The morphology of the units in the legged swarm represents a simplified version of a four-legged locomotor that can move autonomously and interact with the environment using built-in sensing, actuation, and control capabilities. To improve the locomotion performance of individual robots, especially on rough terrain, we added passive flexible components (directionally flexible legs and tail) to the robots' bodies. When the task is relatively simple (e.g., object transport on flat ground) or the task inherently requires a small single unit (e.g., object transport in a narrow tunnel), it is more cost effective to use single robots. However, to solve high-level tasks, such as obstacle traversal and object transport in rough terrain, the units establish physical connections with each other and can organize into a larger multilegged system (Fig. 1).

RESULTS
Single and chained robot experiments
Individual robot design and locomotion test
We hypothesize that legged robots consisting of repeated units (e.g., quadrupeds) could perform tasks in the real world without the need for complex control and sensing. To realize this vision, we equipped each custom-designed quadruped robot (Fig. 2 and movie S1) with three sensors (two touch and one light sensors), an Arduino-based controller, a battery, and passive magnetic connectors (Fig. 2B), allowing the robots to dock each other to form larger morphologies (movie S1).

Quadruped locomotion over rough terrain has been studied by many researchers (24, 34, 66, 67). Several methods based on learning (68–70), optimization (71), and planning (24, 72–74) have been used to design gaits that allow quadrupeds to operate across a variety

Movie 1. Overview of legged swarm system. This video summarizes the structure of terrestrial self-assembled quadruped robots and their individual and swarm capabilities in various environments.

of rough terrains. In this study, we used an open-loop controller—i.e., the control signal (position of servos; fig. S3) sent to the robot does not change at any point in any of the trials—and the control signals would continue to be sent as a function of time and position on the body regardless of external forces or tracking accuracy of the actuators. This simple open-loop controller combined with the mechanics of each individual robot (described below) allows the individual robots to walk in many relatively smooth environments (flat ground, carpet, grass, mulch, leafs, acorns, etc.; Fig. 3 and movie S2) without sensory feedback.

The quadruped robot used in this study (see Materials and Methods) was inspired by insights from our previous study of a hybrid soft/hard myriapod robot (44), which demonstrated how the variation in body/limb forms of myriapods affects the mechanics and performance of terrestrial locomotion. Using the segments of the myriapod robot as a basis, we designed a reconfigurable swarm of identical 3D-printed quadruped robots (Fig. 1 and fig. S1). Each robot has two segments with a single pair of legs on each segment (Fig. 2A). To simplify the mechanical system and reduce the number of actuators, which can be costly in terms of energy and fabrication time, we coupled the horizontal and vertical motions of two legs on a segment with rigid connectors. Two body segments are connected with a body servo that control the lateral body angle (Fig. 2 and fig. S2; Materials and Methods).

All of our robots use a diagonal gait (Fig. 3A and movies S1 and S2) for forward locomotion. In this gait, diagonally opposite legs are in contact with the ground at the same time. The leg moves from front to back in the stance phase (on the ground) and from back to front in the swing phase (in the air). Because the legs are coupled, each leg is on the ground during the half gait cycle. This gait is not statically stable—i.e., the center of mass (CoM) cannot stay within the support polygon at each time step—and the robot flips back during walking and cannot move straight. To improve the stability, we added a passive flexible tail (Fig. 2D and fig. S5). The tail provides an extra support point at the rear and eliminates unwanted turning and flipping. We tested the robot when the tail is active (down) and inactive (up) on two different surfaces: low friction (flat particle board) and high friction (shaggy carpet). On a low-friction surface ($\mu = 0.5$), when the tail is down, the robot walked 9.9 ± 0.6 cm per cycle (5 trials had 29 cycles in total). While the tail is up, it could only move 4.7 ± 0.8 cm per cycle (5 trials had 24 cycles in total) and drifted overall left or right because of instability (Fig. 3B). On a high-friction surface ($\mu = 1$; fig. S4), when the tail is not active (up), the body was substantially inclined (with maximum 25°) and lost ground contact, which resulted in very small forward displacement (1.3 ± 0.3 cm, 5 trials had 15 cycles in total). However, when the tail is active (down), the robot maintained stable walking (fig. S5) with a displacement of 10.3 ± 0.2 cm per cycle (5 trials had 36 cycles in total). Despite variability in the tested environmental conditions, the robots presented a consistent displacement per cycle on both surfaces (Fig. 5A and movie S2).

Most legged robots use position control (75, 76) or torque control (72, 77) to achieve maneuvers on rough terrain, which require a priori information about the terrain and precisely reconstructed trajectories of each joint using feedback from multiple sensors. However, in real-world applications, there are often disturbances, and obtaining noiseless, accurate multisensory feedback is not possible most of the time. To achieve agile, versatile, and robust maneuvers, additional elements are required. Inspired by the highly adaptive locomotion of biological organisms, several studies propose that the control of locomotion on challenging terrain can be
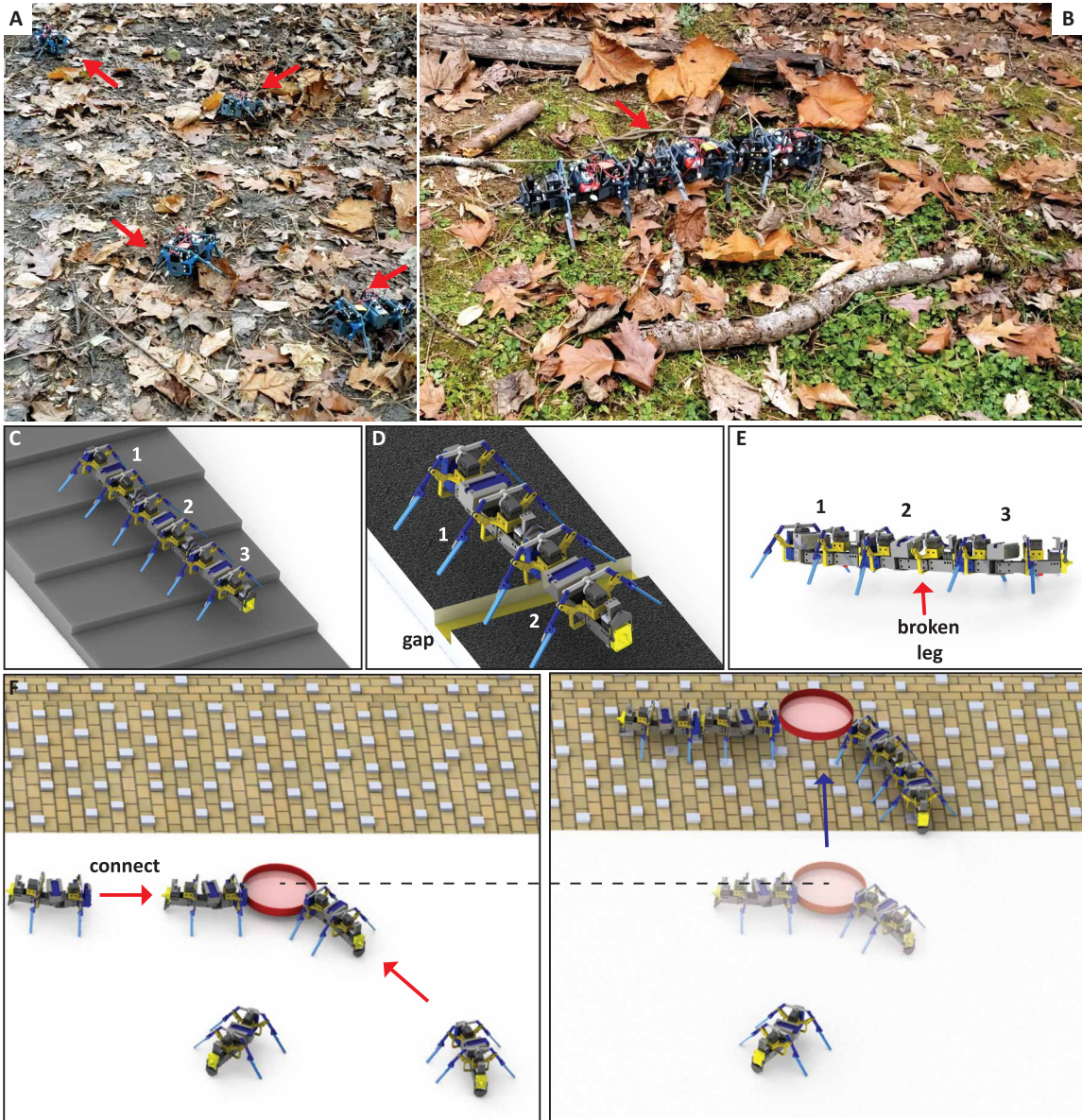
Fig. 1. Terrestrial swarms consisting of chainable legged robots. (**A**) An outdoor demonstration of quadruped swarms (movie S10). The red arrows point to the robots. (**B**) Three robots were chained to traverse over a wooden stick. (**C**) Stair climbing with three chained robots. (**D**) Gap traversal with two chained robots. (**E**) Transporting a broken-legged robot (middle) with the help of two other robots (front and back). (**F**) Quadruped robots connected to create a multilegged robot to achieve object transport in rough terrain.

simplified using passive flexible elements in the locomotive mechanisms (*22*, *44*, *78*, *79*). We improved the complex terrain locomotion capabilities of our robot by adding appropriate mechanical directional compliance to the legs (*44*). The passively directionally flexible leg shown in Fig. 2C consists of two rigid segments (lower and upper), whose total length is equal to 12 cm (movie S1). The leg is stiff when the torque on the joint is positive (counterclockwise) and bends back when the torque is negative (clockwise). The unidirectional rigidity provides enough thrust to move the body forward during the retraction period (ground phase). The directional flexibility creates a more effectively distributed contact area and provides robust obstacle-crossing ability without disturbing the gait (*43*, *44*). Bending usually occurs when the leg is in the air (during the protraction period) and is blocked by an obstacle. After the contact with the obstacle ends, the initial configuration is restored by a helical extension spring attached to the knee joint, which rotates the lower part of the leg (Fig. 2C).

Obstacle traversal

We systematically study the locomotion performance of single and connected multiquadruped robots on various complex environments, including gaps, stairs, and rough terrain with obstacles, namely, complex rough terrain, where the size of the obstacles is on the order of one leg length. Terrains that contain steps and barriers of heights up to 4 cm and gaps of width up to 12 cm push the quadrupedal robots beyond their limits of kinematic feasibility.
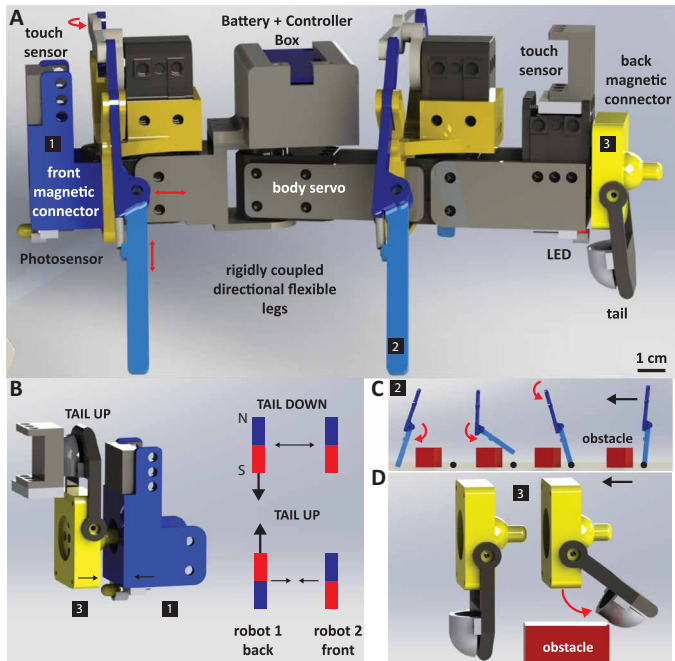
Fig. 2. Elements of the quadruped robot. (**A**) A computer-aided design drawing of a quadruped robot highlighting all main components. The robot includes two segments with one leg pair each. The legs (blue) are out of phase, and their up/down and fore/aft positions are controlled by two different servos (Robotis XL-320). The body servo controls the lateral undulation of the body. The body angle and legs are coupled to each other. The center of the body frame is located at the center of the battery and controller box. The robot is about 22 cm long and weighs 350 g including the battery. A passive tail is attached to the back magnetic connector with a spring, which provides stability during locomotion. The details of parts 1, 2, and 3 are given in (B) to (D). (**B**) Magnetic connection mechanism. Two magnetic connectors (each includes two rare-earth magnets) are attached to the front and the back part of the robot. Two robots can connect to each other when the tail of the front robot is up (movie S1). (**C**) Working principle of the directionally flexible (bends head to tail) leg with a return spring. The black arrow shows the direction of the forward locomotion. The leg approaches the obstacle (red), pivots around the tip (black point), and bends. After it passes the obstacle, the spring returns the leg to its neutral position. (**D**) Flexible tail. The black arrow shows the direction of the forward locomotion.

Fig. 3. The importance of passive tail use on forward locomotion of individual robots using a diagonal gait. (**A**) Leg states (white, in air; black, on ground) and joint angles for a diagonal gait. T represents the gait cycle. All the robots use diagonal gait during the forward and backward locomotion. (**B**) Forward locomotion on a flat surface (particle board) with the passive tail in the air. Blue trajectory shows the CoM trajectory during walking ($n = 4$ cycles). Insets show the side view of the robot and the tip trajectory (pink). (**C**) Forward locomotion on a flat surface (particle board) with the passive tail on the ground. Blue trajectory shows the CoM trajectory during walking ($n = 6$ cycles). White dashed lines show the starting position, and insets show the side view and tip trajectory (pink) of the robot. (**D**) Tail down quadruped walking on natural terrain (grass, acorns, leafs, and mulch; movie S2). An example trajectory (blue, six cycles) of the robot is given in the last image.

1) Gap traversal. Figure 4 (A and B) shows the gap traversal experimental setup (movie S3). In Fig. 4A, a single robot executes forward locomotion and attempts to lunge across a 5-cm gap (about half the length of a robot segment; whole length of the robot is 22 cm). Because the CoM of the robot lies between leg pairs, most of the failures occur after the front legs fall into the gap. In this case, the robot pivots on its hind legs, and the front of the robot pitches forward, which results in an unrecoverable body posture (fig. S6, A and B, and movie S3). Chaining robots together shifts the CoM to the rear and provides a suitable weight distribution to traverse the gap (Fig. 4B). The pitch angle of the body stays close to zero during walking. We calculate the success rate of single and multichained robots over multiple experiments (five trials per case) by changing the width of gaps from 2.5 to 10 cm. A run was deemed a success if the robot crossed the gap and reached the end without falling over.

A single robot could only successfully cross the 2.5-cm gap, whereas two and three connected robots successfully passed the gaps up to 7.5- and 10-cm width, respectively (Table 1). The multichained

robots succeeded with high probability even after slipping or imprecise foot placement; they failed when the front legs fell into the hole and when the edge of the gap's far side was outside of the reachable space of the front legs. Gaps up to 10 cm wide (10 cm equals the distance between two leg pairs) were traversed successfully by three chained robots even if the second pair of legs touched the rear edge of the gap.

2) Stair climbing. Many terrestrial mission scenarios take place in urban settings with stairs, making stair traversal a critical requirement for mobile robots. However, stairs can be challenging obstacles, especially for small, legged robots. Usually, successful stair climbing requires fine-tuning of the hip torque and angle trajectories to particular stair geometries, which requires high-level sensory feedback (80–82). A previous study revealed that increased leg flexibility and half-circular leg geometry offer improved performance in stair climbing (83). We now demonstrate that connected multirobots with directionally
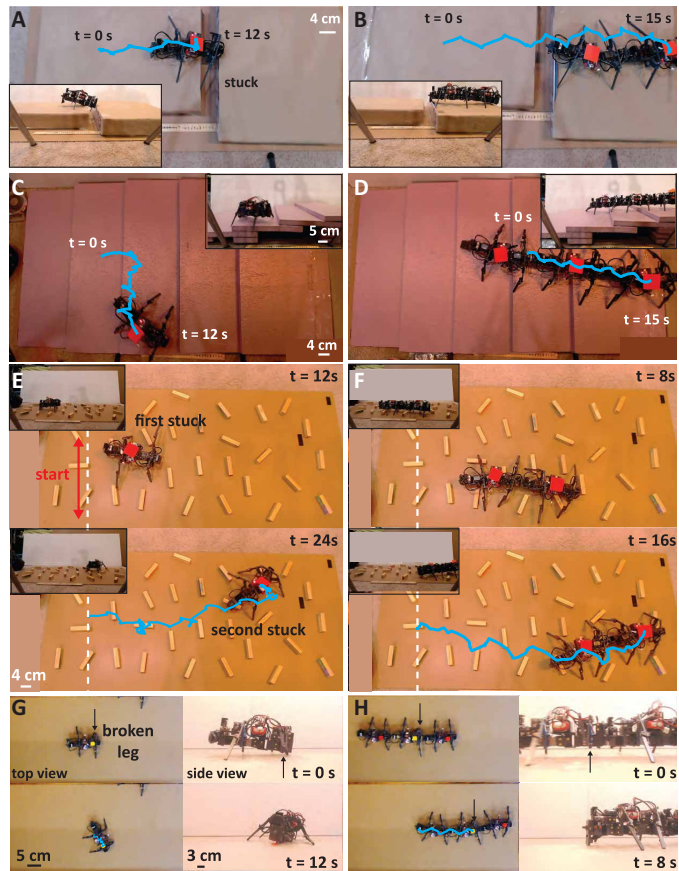
Fig. 4. Obstacle traversal with a single robot and chained devices. (**A**) A single robot becomes stuck in a gap (5 cm). Insets show the side view of the robot. (**B**) Chained two robots pass the same gap successfully. Failure and success numbers of the multiple experiments are given in Table 1 (movie S3). (**C**) A single robot becomes stuck on the first stair and fails to climb it (width = 25 cm and height = 2.5 cm). (**D**) Three chained robots climb the same stairs successfully. The blue trajectories show the CoM movement during the experiment (movie S3). (**E**) Rectangular wooden blocks (length = 7.5, width = 1, and height = 2 cm) were randomly fixed on a particle board (120 cm by 60 cm). White dashed lines show the starting position of the first robots. A single robot became stuck at least once in the course in each experiment (total 20 runs had 32 stuck in total). (**F**) Two chained robots traverse the obstacle course successfully in each experiment (20 runs had 0 stuck). Other insets show the side views of the robots during the experiments. The final CoM trajectories (blue) of the first robots are given in the bottom row (movie S4). (**G**) Snapshots from the experiment where a single robot with a broken right front leg is moving on a flat surface (particle board). The black arrows show the broken leg. The robot rotates to the opposite side of the broken leg. (**H**) Two robots help the broken-legged robot (middle), and they successfully move together (movie S5).

flexible legs can climb steps up to a height of 3 cm (equal to the ground clearance of the body) using an open-loop diagonal walking gait (movie S3).

Figure 4 (C and D) shows the experimental setup that includes five stairs whose width about equals the quadrupedal robot's length, with a height of 2.5 cm. We first tested the performance of a single robot on 1.25- and 2.5-cm-high stairs (movie S3). A single robot could successfully climb 1.25-cm-high stairs with 10.3 ± 1.5 cm per cycle (5 trials had 32 cycles in total). On 2.5-cm-high stairs, in almost all the experiments performed (five trials), one of the rear legs

Table 1. The results of gap traversal experiments with single, two-chained, and three-chained robots (movie S3).

Number of chained robots	GAP SIZE, five runs per case			
	2.5 cm	5 cm	7.5 cm	10 cm
1	All success	All fail	All fail	All fail
2	All success	All success	All success	All fail
3	All success	All success	All success	All success

and the tail became stuck at the first stair, and the single robot turned to the same side as the failed leg. The robot could not generate enough thrust to move the body forward after it became stuck and could only walk on a single stair with a forward displacement of 2.6 ± 1.5 cm per cycle (5 trials had 27 cycles in total). However, when three robots were chained (because many contacting legs can impede maneuverability, we chose three to show an extreme case), although the gaits of individual robots were not coordinated, the chained robots successfully climbed 1.25- and 2.5-cm-high stairs with 7.3 ± 0.3 cm per cycle (5 trials had 47 cycles in total) and 6.9 ± 0.8 cm per cycle (5 trials had 40 cycles in total), respectively (Fig. 5B and movie S3). The directionally flexible leg ensured that the robot's motion remained synchronized with the stairs and the displacement per cycle did not change. However, when we increased the height of the stairs to 3.75 cm (which is higher than the ground clearance of the body), the three-chained robot also failed because the head of the robot became stuck against the stair (fig. S7 and movie S3). If the head was lifted manually (via external assistance), the robot successfully climbed the stairs. For future studies, adding a DoF to the head or body to lift the head or modifying the head shape could mitigate this problem.

3) Rough terrain locomotion. To demonstrate the robustness of multilegged locomotion with flexible legs in a terradynamic scenario of arrays of obstacles, we ran the single robot over scattered wooden rectangular obstacles (height = 2.5 cm, length = 8 cm, and width = 1.5 cm; Fig. 4, E and F; Materials and Methods) attached to a flat board. In this experiment, the robot was again controlled with an open-loop controller without using any sensory feedback. In such terrain, the single robot (quadruped) failed mostly because its tail or legs became stuck and subsequently could not generate enough thrust to elevate the leg or tail to free itself from the obstacle (Fig. 4E). In contrast, the two chained robots created enough robustness to disturbances for successful completion (walking from the beginning to the end of the experimental area) of the runs (Fig. 4F and movie S4). When a directionally flexible leg contacts an obstacle, it bends rearward and crosses the obstacles. This passive leg bending also increases the area of contact, which allows an individual leg to deal with a change of terrain roughness, losing ground contact during the stance phase, or stepping on or hitting an obstacle during the air phase.

We calculate the fraction of the stuck for multiple trials starting from different initial positions. If the robot made no progress in traversing the obstacle after 3 s, the robot was considered stuck. A single robot became stuck at least once in each trials (total 20 trials), whereas the chained multirobots were never stuck in 20 trials (Fig. 5C). This experiment reveals that using the leg adaptation mechanism, open-loop controlled multilegged robots can effectively locomote on terrain with small obstacles without becoming stuck.
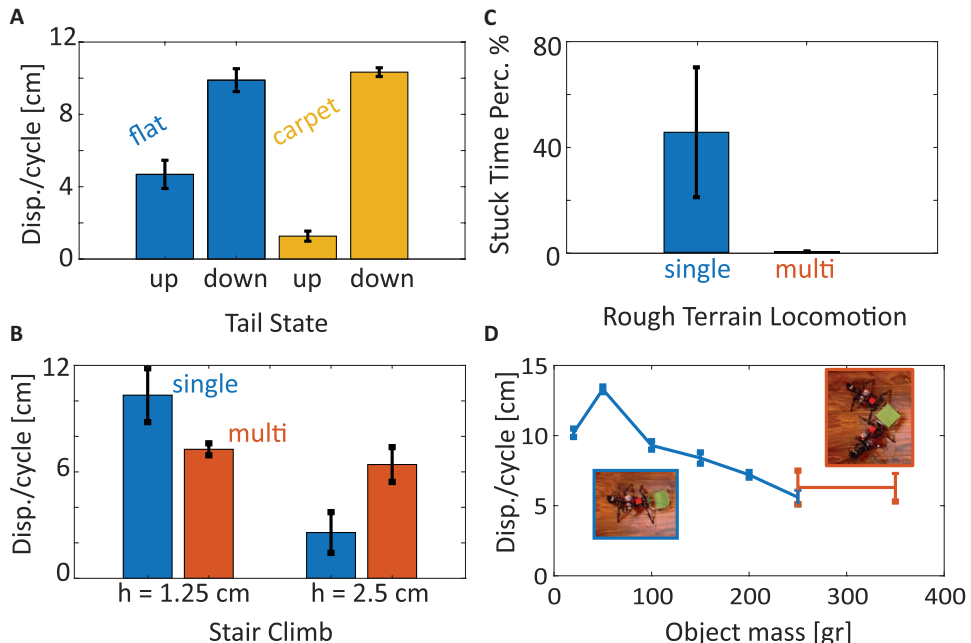
Fig. 5. Performance metrics for obstacle traversal and object transport. (**A**) Mean ± SD CoM displacement per cycle of a single robot with an active (tail down) and nonactive (tail up) on two different surfaces: flat particle board (blue) and carpet (yellow) over multiple experiments (flat-tail up: 5 trials had 24 cycles in total; flat-tail down: 5 trials had 29 cycles in total; carpet-tail up: 5 trials had 15 cycles in total; and carpet-tail down: 5 trials had 36 cycles in total; movie S2). (**B**) Performance of a single (blue) and multichained (red) robots used in stair-climbing experiments given in Fig. 4 (C and D). Mean ± SD CoM displacement per cycle of the first robot in both cases over multiple trials each (five trials each; movie S3). (**C**) The stuck fraction of a single (blue) and two chained (red) robots during the locomotion on rough terrain over multiple trials each (20 trials each). See Fig. 4 (E and F), and movie S4 for experimental details. (**D**) Object transport with a single (blue) and two robots (red). Example CoM trajectories of each robot are given in fig. S10 (movie S8).

Locomotion with broken or missing legs

A previous study (*84*) showed that a miniature centipede robot could walk stably with missing legs without changing its gait if the legs in the front and back segments remained functional. Inspired by this study, we further show that if a single robot fails because of leg loss or other failures, including actuator failure or transmission damage, other robots can help to safely transport it to the desired location. This feature is important for future legged swarm systems where failed robots need to be transported by other robots to a safe location without human intervention.

We disabled the right front leg of one of the robots by removing the lower part of the directionally flexible leg, eliminating any contact of that leg with the ground. Compared with the robot mass (350 g), lower leg masses (2 g) are negligible; therefore, lost leg parts do not affect the mass distribution of the robot. The robot used the same gait (diagonal gait) as in the previous experiments. Every trial for a single quadruped robot resulted in a loss of static stability due to the leg coupling, which resulted in a turning motion and a small forward displacement of 3.2 ± 2 cm per cycle (5 trials had 15 cycles in total; Fig. 4G). When three robots were chained together with the broken legged robot in the middle, they successfully moved straight with a slight increase in performance [11.32 ± 0.1 cm per cycle (5 trials had 24 cycles in total); Fig. 4H] compared with the robots with no missing legs (movie S5). We posit that the slight difference results from the reduced friction caused by the missing leg.

Swarm experiments

In the previous sections, we systematically demonstrated that in our single and chained robots, locomotion could be made robust to environmental disturbances and the robots could navigate through various complex environments. Now, we build on these robophysical studies to demonstrate robot swarm semiautonomous task completion in two relevant and important situations in complex terrain: obstacle (gaps and stairs) traversal via decisions to chain and unchain and object transport over bumpy terrain. We define our swarms as "groups of individuals that join or disconnect to perform a task."

Obstacle traversal

In the first demonstration, the robots seek to reach a target area that has a light source (phototaxis; see Fig. 6A and movie S6 for details). There is an obstacle (stairs) between the target area and the robots. The robots need to traverse (not avoid) the obstacle to reach the target. We used four identical units (quadrupedal robots), one of which (we refer to as the searcher robot) has a higher probability to search the environment.

The searcher robot begins to walk toward the light source, and after $N = 10$ gait cycles (depending on the length of the experimental area, the number of walking cycles can be changed), the robot compares the light intensity measured by a phototransistor mounted on the front bottom part of the robot. The difference between the initial (when the robot is at the beginning of the experimental area) and final light intensities always increases as the robot approaches the light source when there are no obstacles along the way. We measure the approximate light intensity at the robot after 10 cycles when there are not any obstacles along the way and use this number as a threshold for the stair-climbing experiment. After the robot walks 10 gait cycles, if the difference between the initial and final light intensities is below this threshold, the robot stops, moves back 3 cycles, and waits for help by turning on its aid light [bright red light-emitting diode (LED)] attached to the rear end and lifting up its tail for attachment. The three helper robots at the beginning of the experimental area continuously measure the light intensity of the environment. If one of the helper robots receives a light signal from the searcher robot, it automatically becomes active and initiates the search-and-rescue operation.

The first part of the search-and-rescue operation includes the attachment of the two robots. Because the robots only have one light sensor, a single robot measures the light intensity of the environment by turning its body after each gait cycle (see fig. S9D for the description of the turning gaits). It measures the light intensity on its left and right sides and compares them with the light intensity directly in front of it. It turns to the side where it measures maximum light intensity (or stays straight if more light comes from the front).
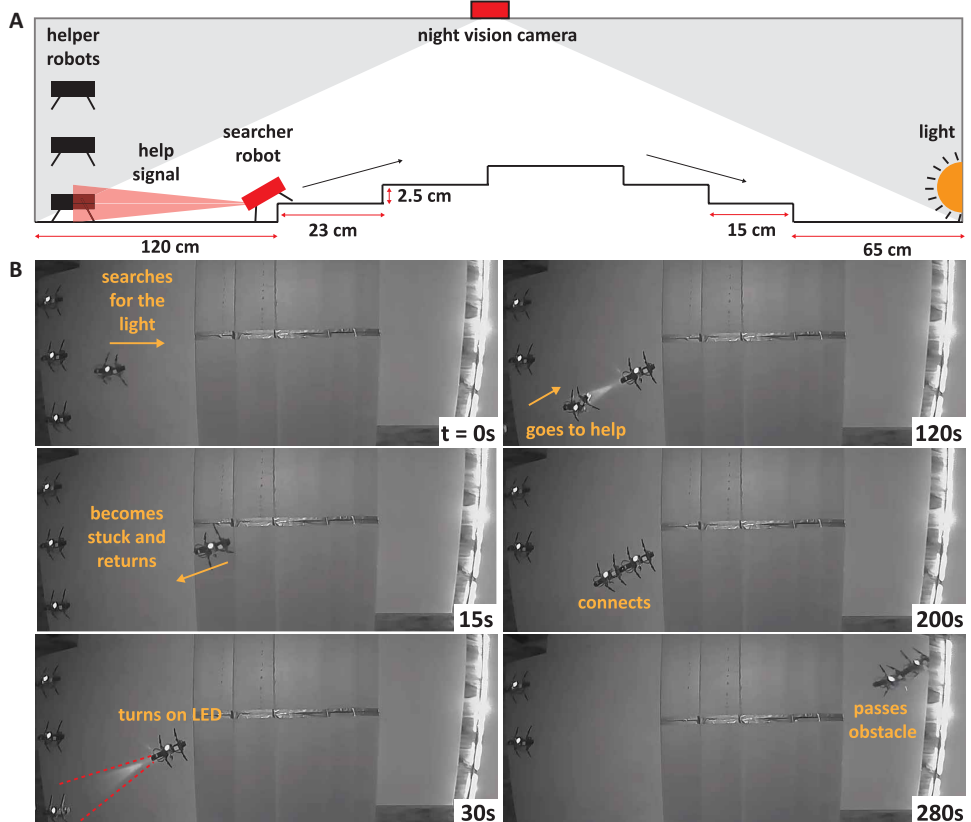
Fig. 6. Autonomous swarm stair climbing. (**A**) Description of the experimental area. Helper robots stay at the beginning of the area. A light source is attached to the other end. A night vision camera (Kasa Spot, KC105) is placed at the top of the arena. (**B**) The searcher robot starts to walk to the light ($t = 0$ s), becomes stuck at the stairs ($t = 15$ s), comes back three cycles, and turns on its aid light ($t = 30$ s). The robot who gets the light signal (bottom robot) starts to search for the stuck robot ($t = 30$ s) and connects to it by following the light gradient of the aid light ($t = 120$ s). After connection, they climb the stairs and disconnect at the end when the front robot get close to the light ($t = 280$ s; movie S6).

After turning, it walks straight for one cycle and repeats the search algorithm until it attaches to the searcher robot (movie S6).

All robots have two touch sensors to detect the connection state: one at the front and one at the backside of the robot. When two robots are chained (in 14 of 20 trials, the robots achieved successful connection; fig. S9, B and C), the dome-shaped pusher attached to the tail touches both the sensors at the tail of the searcher robot and at the head of the helper robot. Although there is no high-level communication (e.g., sending GPS coordinates wirelessly) between robots, the touch sensors allow each robot to know whether it is chained with the other robots. After the robots are chained, they reset their joint angles to a neutral position and start to walk together with the same diagonal gait. They successfully pass the stairs and walk together until the front robot measures high light intensity. After the front robot gets close enough to the light source, it lowers the tail and detaches from the rear robot.

Similar to the stair-climbing experiments, we performed another experiment where the stairs were replaced by the rough terrain used in single and multichained robot experiments (fig. S8). Because the robots are not equipped with any sensor [such as a camera or inertial measurement unit (IMU)] to detect the rough terrain or their own failure, the approximate number of steps ($N = 12$) that the

robot usually becomes stuck is given to the robot externally by the user before the experiment. The searcher robot starts to walk through the obstacle course, and after $N = 12$ cycles, it becomes stuck (with a probability of 80%) and moves back 3 cycles. After that point, similar to the previous experiment, the helper robot finds the searcher robot, and they pass the obstacle area together and detach at the end (movie S6).

Object transport
Collective object transport is a common task (especially in insect societies) where groups of animals solve a high-level task that is not achievable by individuals (such as moving the food particles from one place to another) purely through local interactions among agents and between the agents and the environment (*3*, *4*, *85*). Inspired by a model of ant's foraging behaviors, researchers studied swarming behavior of robots where simple, less expensive, modular units were reconfigured into a team while being as effective as a task-specific, larger, monolithic robot (*85–87*). Using a decentralized control approach, a team of vibrating robots move complex shape objects to the target, which is impossible to achieve individually (*88*). However, most of these studies realized collective transport on a relatively simple environment (flat terrain), which is not applicable and scalable to more complex terradynamic problems (*2*, *88–89*).

Depending on the required task, such as safely and reliably transporting small or large (light or heavy weight) objects when crossing flat or difficult terrain, the number of units involved may vary. For example, on a flat ground, a single robot could easily carry objects (up to $m = 250$ g, about 70% of its mass) that were attached to its head (Fig. 5D; fig. S10, A and B; and movie S8). As the mass of the object was increased, a single robot began to struggle and could not move the object. Increasing the number of the robots that are involved in the task can be a solution (Fig. 5D; figs. S10, C and D, and S11; and movie S8). However, depending on the size and the shape of an object, the dynamics of the transport may change. For example, if the object is too small, robots cannot orient around it without their legs touching each other, resulting in a rotational motion rather than forward transport (fig. S11). In our swarm experiments, we focus on decentralized cooperative manipulation of an object with/without chained robots on a flat ground and rough terrain, without forcing the robots to follow a predefined path.

1) Object transport on flat terrain by pushing without chained connection. We first demonstrate that without a chained connection, the robots can interact with each other through the object that they carry and perform multilegged collective object transport (Fig. 7 and movie S7). This type of collective transport (nonchained) is cost effective when the environment is relatively simple (e.g., flat terrain)
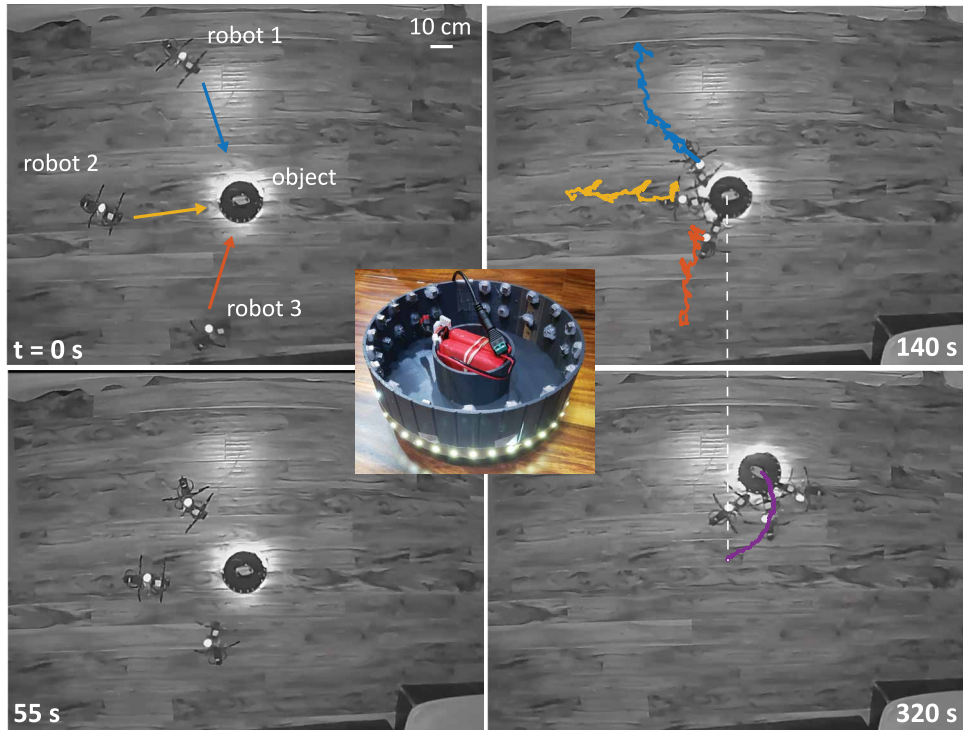
Fig. 7. Swarm object transport on flat terrain. An object (460 g, d = 20 cm) with a light strip around it was placed at the center of the experimental arena. Robots started to search for light (t = 55 s), attached to the object (t = 140 s), and pushed the object collectively (t = 320 s; movie S7).

the shape, weight, and orientation of the object, a legged swarm can transport a circular object to the target (a light source) collectively while traversing rough terrain along the way. In these experiments, initially, two single robots that were strongly attached to the object (d = 25 cm; m = 540 g, 1.5 times heavier than a single robot) with magnets were not able to transfer the object outside of the rough terrain because they could not overcome both the obstacles and static friction (movie S7).

Figure 8 shows snapshots from this experiment where two robots became stuck at the beginning of the rough terrain (Materials and Methods), which means that they could not move the object for more than 5 s (t = 25 s). After that point, the helper robots were attached to the carrier robots, and they collectively transported the object to the outside of the rough terrain (t = 35 to 105 s). During their movement, the robots that were attached directly to the object by lifting continuously measure the light intensity of the environment, and the robot that detected high light intensity detached from the helper robot (t = 120 s) at the end.

Here, we note that because the carried robots were strongly attached to the object, they could not change their relative position to the object. This results in a turning motion if some of the legs of the robots on one side were stuck on obstacles. However, although the robots could not align their forces by orienting their motion toward the light in the obstacle area, they could still move in the direction of the robots that directly see the light source after they passed the obstacle course.

or small robots need to navigate narrow tunnels where they have limited space to move around (fig. S12 and movie S9).

At the beginning of the experiment, three robots were placed away from the circular object (d = 20 cm; 460 g, 1.3 times heavier than a single robot) with an angle of ~90° to each other. To increase the stochasticity of the bonding time, the radial distances between the robots and the object were set to different values. The robots started to search for the object with light around it (Fig. 7; t = 0 s) using the same search method described in the experiment given in Fig. 6. At each gait cycle, the robots measured the light intensity of their left, right, and front sides and went in the direction where the light intensity was greatest until they were very close (defined by the light threshold) to the object (t = 55 s). Robots switched their gait automatically from searching to walking mode after getting close enough to the object (t = 140 s). The 3D-printed object at the center had magnets arranged at 10° intervals around its circumference (see the image at the center of Fig. 7), which allows the robots to loosely bond to the obstacle from any direction. The robots attached to the object began to push it by walking straight. However, because the robots were not attached to the object rigidly, they occasionally lost their connections with the object. In this situation, the robots that were still connected to the object changed the transport direction (the purple trajectory at t = 320 s). During the experiments, we also noticed that the front legs of two robots next to each other were sometimes intertwined. However, this interaction forced the robots to walk synchronously and facilitated the object transport.

2) Object transport over rough terrain by lifting the object with chained connection. Last, we show that without knowledge of the number of units that are involved in the task, properties of the environment, or

DISCUSSION

Existing terrestrial swarms have been largely limited to locomoting on smooth terrain, making these systems inapplicable to real-world problems. In this study, we showed through a series of experiments that a swarm of chainable legged robots is capable of locomoting on challenging environments and accomplishing complex tasks that are not achievable by individual robots. The mechanical design (directional compliance tail and legs) and open-loop gait control strategy allow a single unit to locomote on simple environments (such as flat ground) without any sensory inputs; however, it begins to struggle as the complexity of the environment and tasks become more difficult. The units establish physical connections with each other and can organize into a larger chained multilegged system to solve high-level tasks, such as object transport in rough terrain, traversing gaps, and stairs with limited and imperfect sensing capabilities. The inherent stability and robustness of the multilegged system creates a fault-tolerant legged system.

The minimalist and modular robotic approach that we took in this study can provide a low-cost platform for testing biological hypotheses about mechanical design and movement control strategies. Currently, the robots use the same gait (diagonal gait) in all tested trials. With this gait, a single robot can locomote on various laboratory
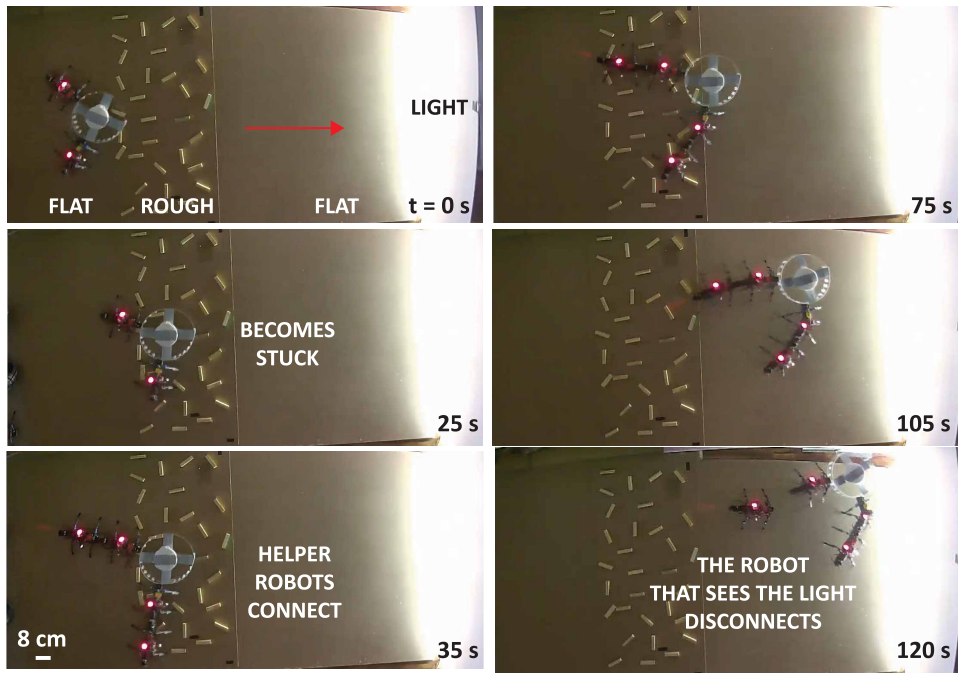
Fig. 8. Swarm object transport over rough terrain by lifting the object. Two robots start to move an object (540 g, $d = 25$ cm, $t = 0$ s). They become stuck in the middle of the rough terrain ($t = 25$ s). Two helper robots are connected manually to each leading robot, and they carry the object near the light source ($t = 35$ to 120 s). The robot that receives high light intensity disconnects from the helper robot ($t = 120$ s).

and natural terrains (movie S2). However, in our previous study (*44*), we showed that leg and body coordination is beneficial (increased speed or stability) for locomoting in different environments. With improved communication between individuals, we expect that the units (quadrupeds) in the swarm could coordinate properly and change their gaits according to environmental conditions or tasks that they perform. With additional sensory inputs, such as IMU, sound, or vision, we expect that they can also autonomously detect and accommodate faults in the swarm, such as locating and moving a broken (mechanically or computationally) robot to a safe location without human intervention or exchanging energy between functioning and faulty robots.

Our study can also be used as a starting point in the development of future robust and cost-effective terrestrial robotic swarms that, like many insect swarms, will be able to collectively traverse challenging environments by creating functional structures (linking their bodies together) without a sophisticated control system. We expect that the findings of our study will enlighten the design of future legged swarms that can adapt to unforeseen situations and perform real-world cooperative tasks, such as search-and-rescue operations, environmental monitoring, collective object transport, and space exploration by taking the advantage of reusability of the simple units, power distribution, and the low cost of construction and maintenance.

MATERIALS AND METHODS
Robot fabrication
All the robot parts were 3D-printed with a Stratasys Dimension Elite printer. Each robot has six Robotis XL-320 servos (stall torque

is 0.39 N · m): five for controlling the body/leg joints and one for controlling the state of the tail. The mechanism that controls the vertical motion of the legs is similar to the four-bar mechanism; the hip joints are hinged to each other using a rigid 1-DoF revolute joint that is connected to the leg up/down servo, whose rotation axis is parallel to the anteroposterior line (fig. S2). The neutral angle of each leg can be modified according to the desired body posture by changing the length of the rigid connector (currently, it is 8 cm) between the legs. Because of the mechanical constraints, the leg for/aft servo can rotate from −25° to 30°, and the body servo can rotate from −30° to 30° from their neutral positions.

The passive directional flexible leg shown in Fig. 2C has two rigid segments (lower and upper), whose total length is equal to 12 cm. The legs can lift up to 30° from their neutral position, which corresponded to a maximum lift about 4 cm above the ground. The vertical distance of the leg pivot joint from the ground ($h_{leg} = 8.5$ cm; fig. S2C) is chosen so that the leg can provide enough leverage from the ground.

Each robot has its own microcontroller (Robotis OpenCM 9.04, 32bit ARM Cortex-M3) and battery (lithium polymer battery, 11.1 V, 1000 mAh) placed in a box that is connected to the body joint. Because the position of the controller + battery box is very close to the CoM of the robot and it is connected to the body joint, it does not affect the balance while the robot is moving.

Each leg and tail has a return spring with a spring constant of 0.2 kg/cm (McMaster; product number, 9654K949). The stiffness of the spring constant is an important parameter. If the springs are too stiff, the legs and tail cannot bend when they encounter obstacles; if it is too soft, the legs bend at the stance phase during normal walking, and the robot cannot stand on its leg.

Each robot is equipped with three sensors. We placed two touch sensors (Robotis TS-10) to the front and back of the robot to detect the connection state of the multiple robots. The front touch sensor is mounted above the front magnetic connector (includes two neodymium rare-earth magnets, 5 mm by 5 mm by 5 mm; K&J Magnetics), and the back touch sensor is mounted above the tail servo. We added a dome-shaped 3D-printed part to the back of the tail (Fig. 2D), which allows the tail to push the front and back touch sensors of the robots when they are connected. The phototransistor light sensor [Adafruit; product identification (ID) number, 2831] at the front and super bright red LED (5 mm, Adafruit; product ID number, 297) at the back are used in light-controlled experiments. To reduce the noise during the autonomous light-controlled connection phase, we inserted both the LED and light sensor into the 3D-printed holder such that the sensor and LED can send and receive the maximum light only when it comes from directly in front of the robot (see Fig. 2, A and B, and fig. S9A for details).

Experimental design and data analysis

All flat-ground experiments were performed on particle boards (120 cm by 120 cm and 120 cm by 60 cm), and carpet experiments were performed on a shaggy area rug (Unique Loom). The gap experiments were performed on two boxes (50 cm by 40 cm by 8 cm) covered with craft paper (ULINE) for uniform friction. The boxes were placed 5.5 cm away from each other. For stair-climbing experiments, we used Foamular insulation foams (Home Depot) and created five stairs 2.5 cm high and 25 cm long. Rough terrain experiments were carried out on a particle board (120 cm by 60 cm) with about 30 rectangular wooden blocks (length = 7.5, width = 1, and height = 2 cm) glued onto the board in a random pattern.

The side and top views of all single and multichained experiments were recorded by two Logitech 920 webcams using Logitech Webcam Software (which allowed synchronized recordings of both views). We placed red tags (4 cm by 4 cm) on each robot for tracking purposes. Light-controlled experiments were done in a dark room, and the trials were recorded by a night vision camera with an internal hard drive (Kasa Spot, KC105).

The beam angle of an aid LED attached to the back of the robot is 10° (see fig. S9A for beam angle and beam field). During the experiments, if all of the helper robots were outside the beam field of the searcher robot (meaning that all of the robots could not see the searcher robot), we repeated those trials.

In swarm experiments, we covered the end of the experimental area with a foam board with ultrabright flexible LED strips (12 V) attached to it. The swarm object transport experiments were done with two different circular boxes. The first one (d = 20 cm and m = 460 g) was 3D-printed with a Stratasys Dimension Elite printer. Seventy-two neodymium rare-earth magnets arranged at 10° intervals were hot-glued to the inside of the box in an opposite orientation to the front magnetic connectors of the robots. A flexible LED strip was attached to the bottom edge, and it was powered with a 11.1-V 1000-mA LB-010 LiPo battery. To balance the CoM of the object, we used another battery as a counterweight. Object transport on flat terrain experiments were performed on a hardwood floor. The second object was made with a thin acrylic sheet (85 cm by 8 cm) to provide a clear view for the robot during the light search. A mass (~300 g) was fixed to the center of the acrylic box to increase the weight. All video analyses (color tracking) were done by the MATLAB Image Processing Toolbox.

SUPPLEMENTARY MATERIALS

robotics.sciencemag.org/cgi/content/full/6/56/eabf1628/DC1
Figs. S1 to S12
Movies S1 to S10

REFERENCES AND NOTES

1. T. D. Seeley, S. C. Buhrman, Nest-site selection in honey bees: How well do swarms implement the "best-of-N" decision rule? *Behav. Ecol. Sociobiol.* **49**, 416–427 (2001).
2. C. R. Kube, E. Bonabeau, Cooperative transport by ants and robots. *Robot. Auton. Syst.* **30**, 85–101 (2000).
3. H. F. Mccreery, Z. A. Dix, M. D. Breed, R. Nagpal, Collective strategy for obstacle navigation during cooperative transport by ants. *J. Exp. Biol.* **219**, 3366–3375 (2016).
4. O. Feinerman, I. Pinkoviezky, A. Gelblum, E. Fonio, N. S. Gov, The physics of cooperative transport in groups of ants. *Nat. Phys.* **14**, 683–693 (2018).
5. C. Anderson, G. Theraulaz, J. L. Deneubourg, Self-assemblages in insect societies. *Insectes Soc.* **49**, 99–110 (2002).
6. J. S. Turner, Termites as models of swarm cognition. *Swarm Intelligence* **5**, 19–43 (2011).
7. C. K. Hemelrijk, H. Hildenbrandt, Schools of fish and flocks of birds: Their shape and internal structure by self-organization. *Interface Focus* **6**, 726–737 (2012).
8. A. Okubo, Dynamical aspects of animal grouping: Swarms, schools, flocks, and herds. *Adv. Biophys.* **22**, 1–94 (1986).
9. M. Brambilla, E. Ferrante, M. Birattari, M. Dorigo, Swarm robotics: A review from the swarm engineering perspective. *Swarm Intelligence* **7**, 1–41 (2013).
10. A. Kushleyev, D. Mellinger, C. Powers, V. Kumar, Towards a swarm of agile micro quadrotors. *Autonomous Robots* **35**, 287–300 (2013).
11. M. Schranz, M. Umlauft, M. Sende, W. Elmenreich, Swarm robotic behaviors and current applications. *Front. Robot. AI* **7**, 36 (2020).
12. S. J. Chung, A. A. Paranjape, P. Dames, S. Shen, V. Kumar, A survey on aerial swarm robotics. *IEEE Trans. Robot.* **34**, 837–855 (2018).
13. N. Nedjah, L. S. Junior, Review of methodologies and tasks in swarm robotics towards standardization. *Swarm Evol. Comput.* **50**, 100565 (2019).
14. M. Raibert, *Legged Robots That Balance* (MIT Press, 2000).
15. L. Ding, Z. Deng, H. Gao, K. Nagatani, K. Yoshida, L. Ding, Z. Deng, H. Gao, K. Nagatani, K. Yoshida, Planetary rovers' wheel-soil interaction mechanics: new challenges and applications for wheeled mobile robots. *Intell. Serv. Robot.* **4**, 17–38 (2011).
16. E. Guizzo, E. Ackerman, The hard lessons of DARPA's robotics challenge. *IEEE Spectrum* **8**, 52 (2015).
17. C. Li, T. Zhang, D. I. Goldman, A terradynamics of legged locomotion on granular media. *Science* **339**, 1408–1412 (2013).
18. R. W. Blob, T. E. Higham, Terrestrial locomotion-where do we stand, where are we going? An introduction to the symposium. *Integr. Comp. Biol.* **54**, 1051–1057 (2014).
19. T. Weihmann, Leg force interference in polypedal locomotion. *Sci. Adv.* **4**, eaat3721 (2018).
20. A. J. Ijspeert, Amphibious and sprawling locomotion: From biology to robotics and back. *Annu. Rev. Control Robot. Autonom. Syst.* **3**, 173–193 (2020).
21. R. Othayoth, G. Thoms, C. Li, An energy landscape approach to locomotor transitions in complex 3D terrain. *Proc. Natl. Acad. Sci. U.S.A.* **117**, 14987–14995 (2020).
22. U. Saranli, M. Buehler, D. E. Koditschek, RHex: A simple and highly mobile hexapod robot. *Int. J. Robot. Res.* **20**, 616–631 (2001).
23. M. Raibert, K. Blankespoor, G. Nelson, R. Playter, Bigdog, the rough-terrain quadruped robot, in *Proceedings of the 17th IFAC World Congress* (IFAC, 2008), vol. 41, pp. 10822–10825.
24. P. Fankhauser, M. Bjelonic, C. D. Bellicoso, T. Miki, M. Hutter, Robust Rough-Terrain Locomotion with a Quadrupedal Robot, in *IEEE International Conference on Robotics and Automation* (ICRA, 2018), pp.5761–5768.
25. R. J. Full, M. S. Tu, Mechanics of a rapid running insect: two-, four- and six-legged locomotion. *J. Exp. Biol.* **156**, 215–231 (1991).
26. C. F. Herreid, D. A. Prawel, R. J. Full, Energetics of running cockroaches. *Science* **212**, 331–333 (1981).
27. R. J. Full, D. R. Stokes, A. N. Ahn, R. K. Josephson, Energy absorption during running by leg muscles in a cockroach. *J. Exp. Biol.* **201**, 997–1012 (1998).
28. J. T. Watson, R. E. Ritzmann, S. N. Zill, A. J. Pollack, Control of obstacle climbing in the cockroach, blaberus discoidalis. I. Kinematics. *J. Comp. Physiol. A Neuroethol. Sens. Neural. Behav. Physiol.* **188**, 39–53 (2002).
29. W. A. Lewinger, C. M. Harley, M. S. Watson, M. S. Branicky, R. E. Ritzmann, R. D. Quinn, Animal-inspired sensing for autonomously climbing or avoiding obstacles. *Appl. Bionics Biomech.* **6**, 43–61 (2009).
30. D. I. Goldman, T. S. Chen, D. M. Dudek, R. J. Full, Dynamics of rapid vertical climbing in cockroaches reveals a template. *J. Exp. Biol.* **209**, 2990–3000 (2006).
31. J. T. Watson, R. E. Ritzmann, A. J. Pollack, Control of climbing behavior in the cockroach, blaberus discoidalis. II. motor activities associated with joint movement. *J. Comp. Physiol. A Neuroethol. Sens. Neural. Behav. Physiol.* **188**, 55–69 (2002).
32. P. J. Csonka, K. J. Waldron, *A Brief History of Legged Robotics* (Springer Netherlands, 2011), pp. 59–73.
33. M. Kalakrishnan, J. Buchli, P. Pastor, M. Mistry, S. Schaal, Fast, robust quadruped locomotion over challenging terrain, in *Proceedings - IEEE International Conference on Robotics and Automation* (IEEE, 2010), pp. 2665–2670.
34. J. Lee, J. Hwangbo, L. Wellhausen, V. Koltun, M. Hutter, Learning quadrupedal locomotion over challenging terrain. *Sci. Robot.* **5**, eabc5986 (2020).
35. F. Farshidian, M. Neunert, A. W. Winkler, G. Rey, J. Buchli, An efficient optimal planning and control framework for quadrupedal locomotion, in *Proceedings - IEEE International Conference on Robotics and Automation* (IEEE, 2017), pp. 93–100.
36. S. Seok, A. Wang, M. Y. Chuah, D. Otten, J. Lang, S. Kim, Design principles for highly efficient quadrupeds and implementation on the MIT Cheetah robot, in *Proceedings - IEEE International Conference on Robotics and Automation* (IEEE, 2013), pp. 3307–3312.
37. F. Jenelten, J. Hwangbo, F. Tresoldi, C. D. Bellicoso, M. Hutter, Dynamic locomotion on slippery ground. *IEEE Robot. Autom. Lett.* **4**, 4170–4176 (2019).
38. A. Cully, J. Clune, D. Tarapore, J. B. Mouret, Robots that can adapt like animals. *Nature* **521**, 503–507 (2015).
39. S. M. LaValle, *Planning Algorithms* (Cambridge Univ. Press, 2006).

40. J. R. Rebula, P. D. Neuhaus, B. V. Bonnlander, M. J. Johnson, J. E. Pratt, A controller for the Littledog quadruped walking on rough terrain, in *Proceedings 2007 IEEE International Conference on Robotics and Automation* (IEEE, 2007), pp. 1467–1473.

41. I. R. Manchester, U. Mettin, F. Iida, R. Tedrake, Stable dynamic walking over uneven terrain. *Int. J. Robot. Res.* **30**, 265–279 (2011).

42. D. Pongas, M. Mistry, and S. Schaal, A robust quadruped walking gait for traversing rough terrain, in *Proceedings 2007 IEEE International Conference on Robotics and Automation* (IEEE, 2007), pp. 1474–1479.

43. J. C. Spagna, D. I. Goldman, P.-C. Lin, D. E. Koditschek, R. J. Full, Distributed mechanical feedback in arthropods and robots simplifies control of rapid running on challenging terrain. *Bioinspir. Biomim.* **2**, 9–18 (2007).

44. Y. Ozkan-Aydin, B. Chong, E. Aydin, and D. I. Goldman, A systematic approach to creating terrain-capable hybrid soft/hard myriapod robots, in *2020 3rd IEEE International Conference on Soft Robotics (RoboSoft)* (IEEE, 2020), pp. 156–163.

45. C. R. Reid, M. J. Lutz, S. Powell, A. B. Kao, I. D. Couzin, S. Garnier, Army ants dynamically adjust living bridges in response to a cost-benefit trade-off. *Proc. Natl. Acad. Sci. U.S.A.* **112**, 15113–15118 (2015).

46. T. D. Seeley, S. Camazine, J. Sneyd, Collective decision-making in honey bees: How colonies choose among nectar sources. *Behav. Ecol. Sociobiol.* **28**, 277–290 (1991).

47. H. Wei, Y. Chen, M. Liu, Y. Cai, T. Wang, Swarm robots: From self-assembly to locomotion. *Comput. J.* **54**, 1465–1474 (2011).

48. M. Divband Soorati, M. K. Heinrich, J. Ghofrani, P. Zahadat, H. Hamann, Photomorphogenesis for robot self-assembly: Adaptivity, collective decision-making, and self-repair. *Bioinspir. Biomim.* **14**, 056006 (2019).

49. H. Wei, Y. Chen, J. Tan, T. Wang, Sambot: A self-assembly modular robot system. *IEEE ASME Trans. Mechatron.* **16**, 745–757 (2011).

50. M. Dorigo, V. Trianni, E. Şahin, R. Groß, T. H. Labella, G. Baldassarre, S. Nolfi, J. L. Deneubourg, F. Mondada, D. Floreano, L. M. Gambardella, Evolving self-organizing behaviors for a swarm-bot. *Auton. Robot.* **17**, 223–245 (2004).

51. M. Rubenstein, A. Cornejo, R. Nagpal, Programmable self-assembly in a thousand-robot swarm. *Science* **345**, 795–799 (2014).

52. M. Yim, K. Roufas, D. Duff, Y. Zhang, C. Eldershaw, S. Homans, Modular reconfigurable robots in space applications. *Auton. Robot.* **14**, 225–237 (2003).

53. M. Yim, W. M. Shen, B. Salemi, D. Rus, M. Moll, H. Lipson, E. Klavins, G. S. Chirikjian, Modular self-reconfigurable robot systems [Grand challenges of robotics]. *IEEE Robot. Autom. Mag.* **14**, 43–52 (2007).

54. K. Gilpin, D. Rus, Modular robot systems. *IEEE Robot. Autom. Mag.* **17**, 38–55 (2010).

55. P. Moubarak, P. Ben-Tzvi, Modular and reconfigurable mobile robotics. *Rob. Auton. Syst.* **60**, 1648–1663 (2012).

56. A. Brunete, A. Ranganath, S. Segovia, J. P. de Frutos, M. Hernando, E. Gambao, Current trends in reconfigurable modular robots design. *Int. J. Adv. Robot. Syst.* **14**, 1–21 (2017).

57. P. J. White, K. Kopanski, H. Lipson, Stochastic self-reconfigurable cellular robotics, in *Proceedings - IEEE International Conference on Robotics and Automation* (IEEE, 2004), vol. 2004, pp. 2888–2893.

58. P. White, V. Zykov, J. C. Bongard, H. Lipson, Three dimensional stochastic reconfiguration of modular robots. in *Proc. Robot. Sci. Syst.*, (2005), pp. 161–168 .

59. S. Li, R. Batra, D. Brown, H. D. Chang, N. Ranganathan, C. Hoberman, D. Rus, H. Lipson, Particle robotics based on statistical mechanics of loosely coupled components. *Nature* **567**, 361–365 (2019).

60. W. Savoie, T. A. Berrueta, Z. Jackson, A. Pervan, R. Warkentin, S. Li, T. D. Murphey, K. Wiesenfeld, D. I. Goldman, A robot made of robots: Emergent transport and control of a smarticle ensemble. *Sci. Robot.* **4**, eaax4316 (2019).

61. R. Groß, M. Bonani, F. Mondada, M. Dorigo, Autonomous self-assembly in swarm-bots. *IEEE Trans. Robot.* **22**, 1115–1130 (2006).

62. R. O'Grady, A. L. Christensen, M. Dorigo, Self-assembly and morphology control in a swarm-bot, in *IEEE International Conference on Intelligent Robots and Systems* (IEEE, 2007), pp. 2551–2552.

63. F. Mondada, G. C. Pettinaro, A. Guignard, I. W. Kwee, D. Floreano, J. L. Deneubourg, S. Nolfi, L. M. Gambardella, M. Dorigo, Swarm-bot: A new distributed robotic concept. *Auton. Robot.* **17**, 193–221 (2004).

64. J. Aguilar, T. Zhang, F. Qian, M. Kingsbury, B. McInroe, N. Mazouchova, C. Li, R. Maladen, C. Gong, M. Travers, R. L. Hatton, H. Choset, P. B. Umbanhowar, D. I. Goldman, A review on locomotion robophysics: The study of movement at the intersection of robotics, soft matter and dynamical systems. *Rep. Prog. Phys.* **79**, 110001 (2016).

65. Y. Ozkan-Aydin, J. M. Rieser, C. M. Hubicki, W. Savoie, D. I. Goldman, Physics approaches to natural locomotion: Every robot is an experiment, in *Robotic Systems and Autonomous Platforms*, S. M. Walsh, M. S. Strano, Eds., Woodhead Publishing in Materials, (Woodhead Publishing, 2019) pp. 109–127.

66. M. Kalakrishnan, J. Buchli, P. Pastor, M. Mistry, S. Schaal, Learning, planning, and control for quadruped locomotion over challenging terrain. *Int. J. Robot. Res.* **30**, 236–258 (2011).

67. Y. Fukuoka, H. Kimura, A. H. Cohen, Adaptive dynamic walking of a quadruped robot on irregular terrain based on biological concepts. *Int. J. Robot. Res.* **22**, 187–202 (2003).

68. H. Lee, Y. Shen, C. H. Yu, G. Singh, A. Y. Ng, Quadruped robot obstacle negotiation via reinforcement learning, in *Proceedings - IEEE International Conference on Robotics and Automation* (IEEE, 2006), vol. 2006, 3003–3010.

69. M. A. Zucker, N. M. Ratliff Stolle, J. Chestnutt, J. A. Bagnell, N. Ratliff, M. Stolle, J. Chestnutt, J. A. Bagnell, C. G. Atkeson, J. Kuffner, A. A. A. M. Zucker, M. Zucker, N. Ratliff, M. Stolle, J. Chestnutt, J. A. Bagnell, C. G. Atkeson, J. Kuffner, Optimization and learning for rough terrain legged locomotion. *Int. J. Robot. Res.* **30**, 175–191 (2011).

70. J. Zico Kolter, A. Y. Ng, The Stanford LittleDog: A learning and rapid replanning approach to quadruped locomotion. *Int. J. Robot. Res.* **30**, 150–174 (2011).

71. M. Zucker, J. A. Bagnell, C. G. Atkeson, J. Kuffner, An optimization approach to rough terrain locomotion, in *Proceedings - IEEE International Conference on Robotics and Automation* (IEEE, 2010), pp. 3589–3595.

72. J. Buchli, M. Kalakrishnan, M. Mistry, P. Pastor, S. Schaal, Compliant quadruped locomotion over rough terrain, in *2009 IEEE/RSJ International Conference on Intelligent Robots and Systems* (IEEE, 2009), vol. 12, pp. 814–820.

73. M. Focchi, R. Orsolino, M. Camurri, V. Barasuol, C. Mastalli, D. G. Caldwell, C. Semini, Heuristic planning for rough terrain locomotion in presence of external disturbances and variable perception quality, in *Springer Tracts in Advanced Robotics* , A. Grau, Y. Morel, A. Puig-Pey, F. Cecchi, Eds. (Springer, 2020), pp. 165–209.

74. C. Mastalli, I. Havoutis, M. Focchi, D. G. Caldwell, C. Semini, Motion planning for quadrupedal locomotion: Coupled planning, terrain mapping and whole-body control. *IEEE Trans. Robot.* **36**, 1635–1648 (2020).

75. D. A. Messuri, C. A. Klein, Automatic body regulation for maintaining stability of a legged vehicle during rough-terrain locomotion. *IEEE J. Robot. Autom.* **1**, 132–141 (1985).

76. K. Hauser, T. Bretl, J.-C. Latombe, K. Harada, B. Wilcox, Motion planning for legged robots on varied terrain. *Int. J. Robot. Res.* **27**, 1325–1349 (2008).

77. M. Focchi, A. del Prete, I. Havoutis, R. Featherstone, D. G. Caldwell, C. Semini, High-slope terrain locomotion for torque-controlled quadruped robots. *Auton. Robot.* **40**, 259–272 (2017).

78. K. S. Espenschied, R. D. Quinn, R. D. Beer, H. J. Chiel, Biologically based distributed control and local reflexes improve rough terrain locomotion in a hexapod robot. *Robot. Auton. Syst.* **18**, 59–64 (1996).

79. K. L. Hoffman, Design and locomotion studies of a miniature centipede-inspired robot, thesis (Harvard University, Cambridge, MA, 2013).

80. M. Buehler, R. Battaglia, A. Cocosco, G. Hawker, J. Sarkis, K. Yamazaki, SCOUT: A simple quadruped that walks, climbs, and runs, in *Proceedings - IEEE International Conference on Robotics and Automation* (IEEE, 1998), pp. 1707–1712.

81. C. C. Ko, S. C. Chen, C. H. Li, P. C. Lin, Trajectory planning and four-leg coordination for stair climbing in a quadruped robot, in *IEEE/RSJ 2010 International Conference on Intelligent Robots and Systems, IROS 2010 - Conference Proceedings* (IEEE, 2010), pp. 5335–5340.

82. A. M. Johnson, M. T. Hale, G. C. Haynes, D. E. Koditschek, Autonomous legged hill and stairwell ascent, in *9th IEEE International Symposium on Safety, Security, and Rescue Robotics, SSRR 2011* (IEEE, 2011), pp. 134–142.

83. E. Z. Moore, D. Campbell, F. Grimminger, M. Buehler, Reliable stair climbing in the simple hexapod 'RHex', in *Proceedings - IEEE International Conference on Robotics and Automation* (IEEE, 2002), vol. 3, pp. 2222–2227.

84. K. L. Hoffman, R. J. Wood, Robustness of centipede-inspired millirobot locomotion to leg failures, in *2013 IEEE/RSJ International Conference on Intelligent Robots and Systems* (IEEE, 2013), pp. 1472–1479.

85. S. Berman, Q. Lindsey, M. S. Sakar, V. Kumar, S. C. Pratt, Experimental study and modeling of group retrieval in ants as an approach to collective transport in swarm robotic systems, in *Proceedings of the IEEE* (IEEE, 2011), vol. 99, pp. 1470–1481.

86. M. J. Krieger, J. B. Billeter, L. Keller, Ant-like task allocation and recruitment in cooperative robots. *Nature* **406**, 992–995 (2000).

87. R. Groß, E. Tuci, M. Dorigo, M. Bonani, F. Mondada, Object transport by modular robots that self-assemble, in *Proceedings - IEEE International Conference on Robotics and Automation* (IEEE, 2006), vol. 2006, 2558–2564.

88. M. Rubenstein, A. Cabrera, J. Werfel, G. Habibi, J. McLurkin, R. Nagpal, Collective transport of complex objects by simple robots, in *Proceedings of the 2013 International Conference on Autonomous Agents and Multi-agent Systems* (AMAS, 2013), pp. 47–54.

89. E. Tuci, R. Gross, V. Trianni, F. Mondada, M. Bonani, M. Dorigo, Cooperation through self-assembly in multi-robot systems. *ACM Trans. Auton. Adapt. Syst.* **1**, 115–150 (2006).

Citation: Y. Ozkan-Aydin, D. I. Goldman, Self-reconfigurable multilegged robot swarms collectively accomplish challenging terradynamic tasks. *Sci. Robot.* **6**, eabf1628 (2021).

Science Robotics

Self-reconfigurable multilegged robot swarms collectively accomplish challenging terradynamic tasks

Yasemin Ozkan-Aydin and Daniel I. Goldman

ARTICLE TOOLS	http://robotics.sciencemag.org/content/6/56/eabf1628
SUPPLEMENTARY MATERIALS	http://robotics.sciencemag.org/content/suppl/2021/07/26/6.56.eabf1628.DC1
RELATED CONTENT	http://robotics.sciencemag.org/content/robotics/4/34/eaax4316.full http://science.sciencemag.org/content/sci/339/6126/1408.full
REFERENCES	This article cites 60 articles, 10 of which you can access for free http://robotics.sciencemag.org/content/6/56/eabf1628#BIBL
PERMISSIONS	http://www.sciencemag.org/help/reprints-and-permissions

Use of this article is subject to the Terms of Service

Supplementary Materials for

Self-reconfigurable multilegged robot swarms collectively accomplish challenging terradynamic tasks

Yasemin Ozkan-Aydin and Daniel I. Goldman

Corresponding author: Yasemin Ozkan-Aydin, yesminozkan@gmail.com

This PDF file includes:

Figs. S1 to S12

Other Supplementary Material for this manuscript includes the following:

Movies S1 to S10

Supplementary Figures
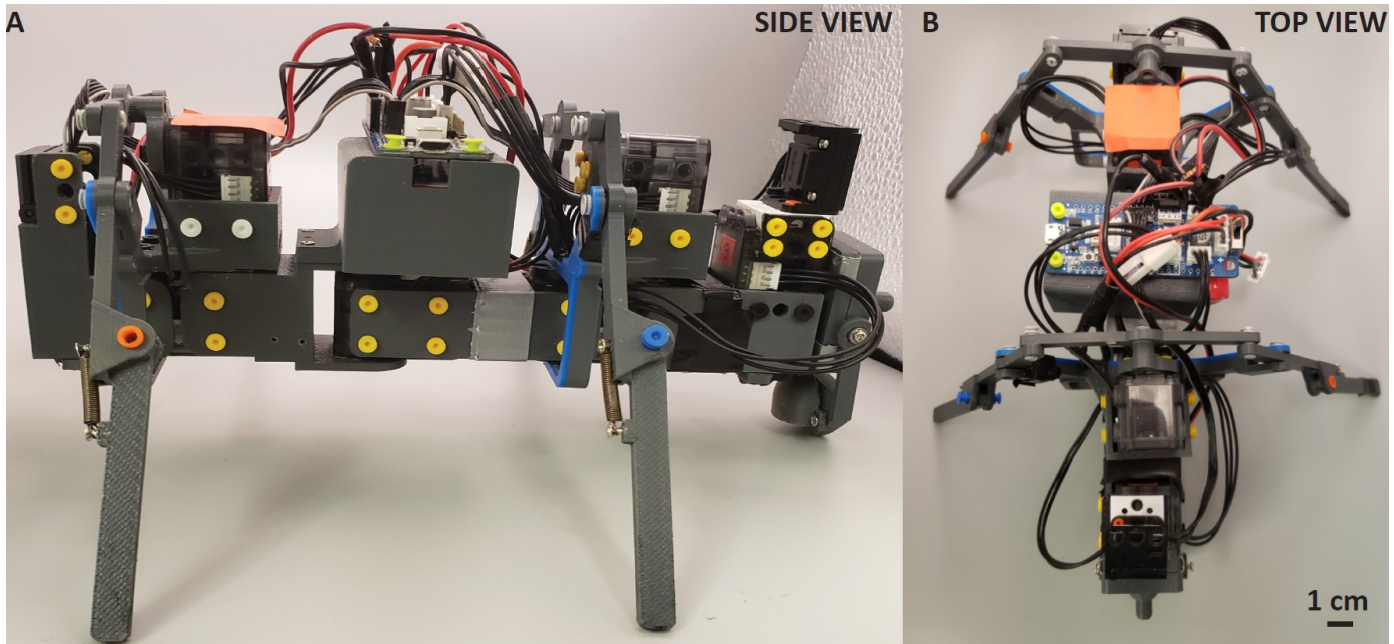
Figure S1: Side and top view of a single robot. A. Side view, **B.** Top view.
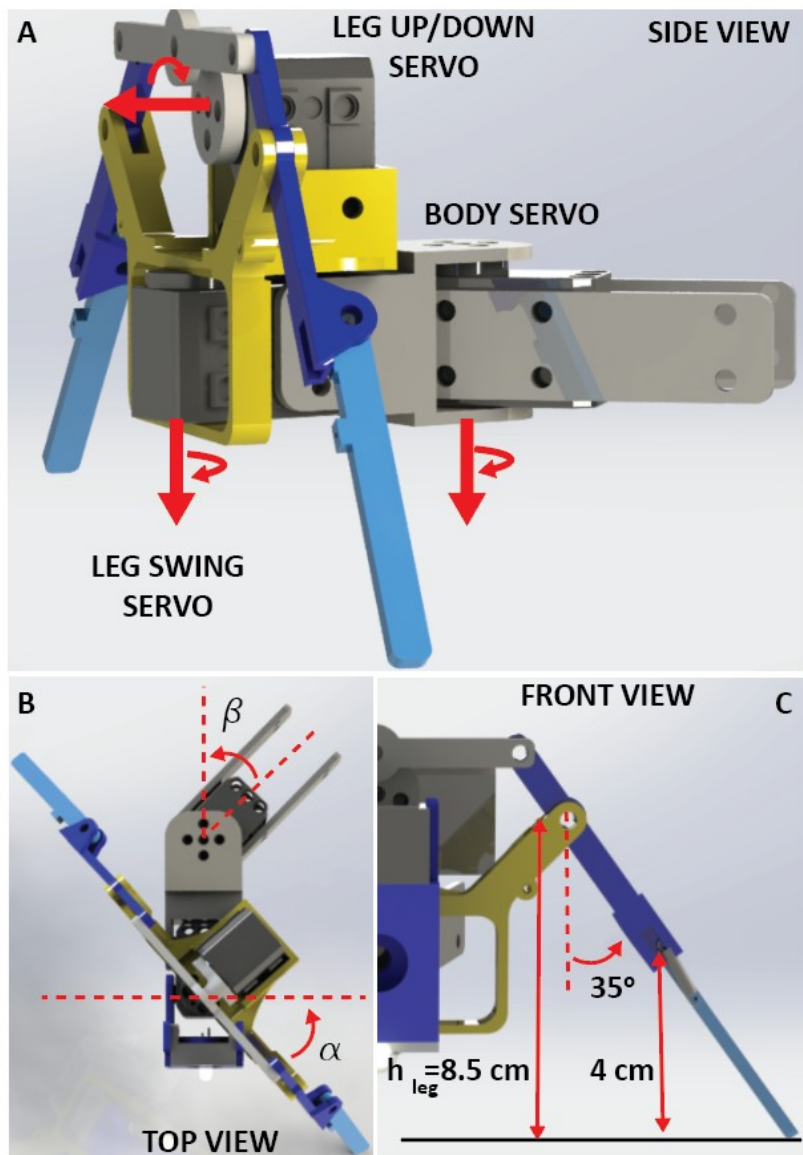
Figure S2: Definition of the robot servo and leg angles. A. Rotation axis of the three servos (leg up/down, leg swing and body) in one segment. **B.** Top view of the body(β) and leg swing angle (α). **C.** The legs are oriented 35° from the vertical plane (neutral position).
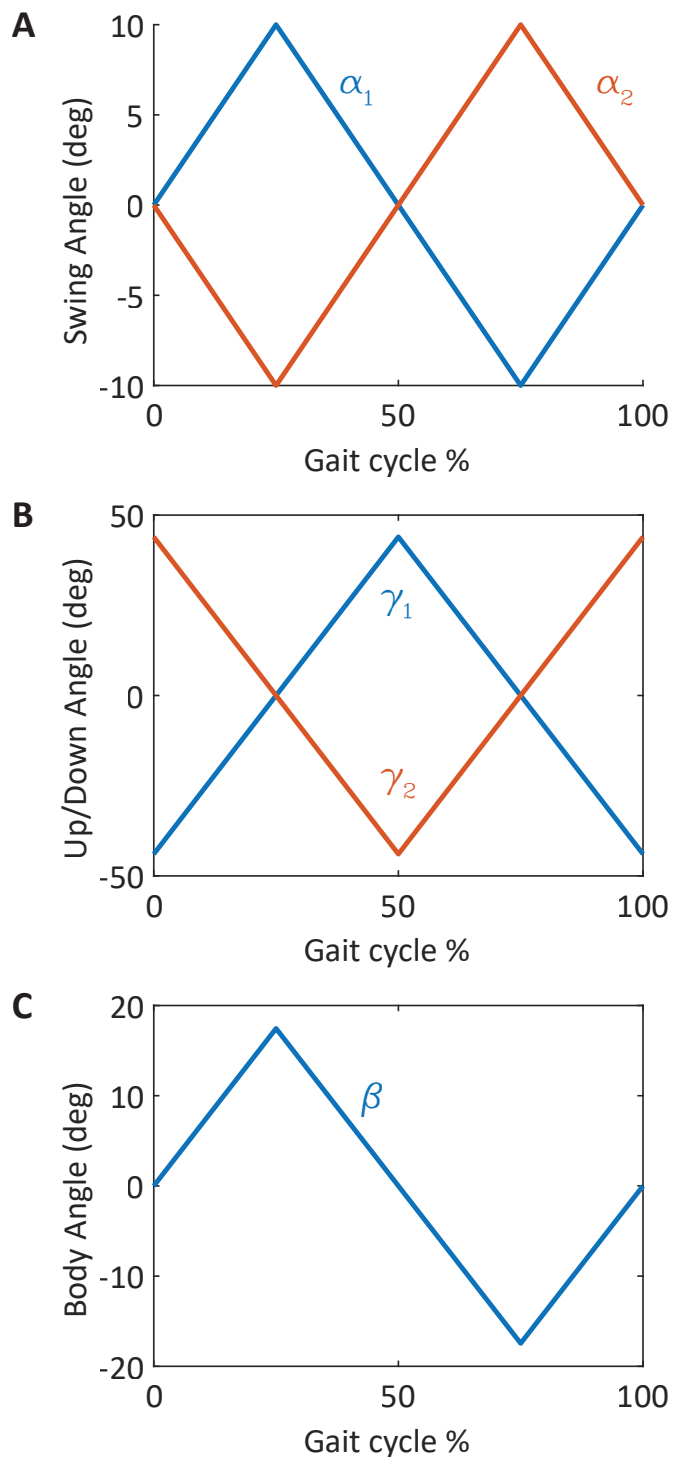
Figure S3: Commanded leg and body angles during the forward walking. A. The swing angle of the leg pairs at the first (α_1) and second (α_2) segment, **B.** The up/down angle of the leg pairs at the first (γ_1) and second (γ_2) segment, **C.** Body angle. Zero degree means the neutral position of the joint angle (see Fig. S2B for the definition of the angles).
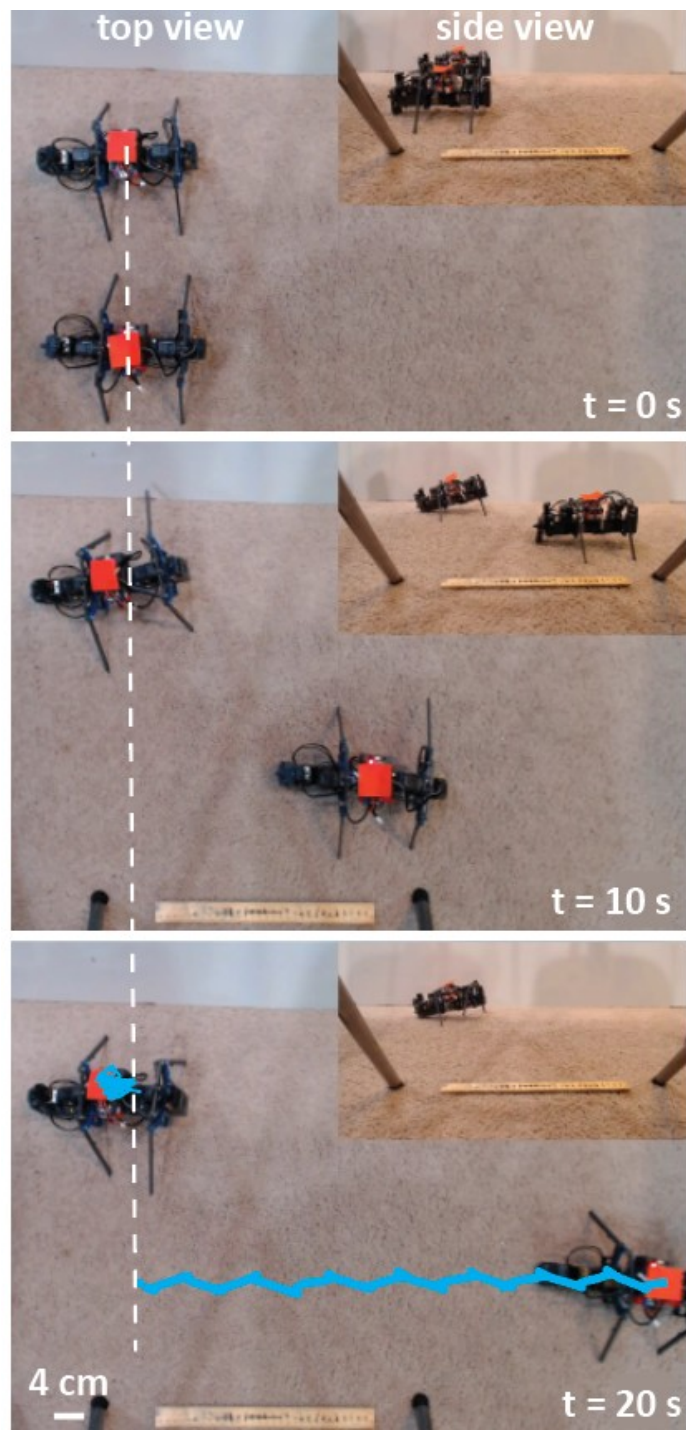
Figure S4: Tail up and down locomotion on high friction surface carpet. Two robots (top: tail up, down: tail down) moving on a shaggy carpet for 20 sec. The trajectories of the center of mass are given in the last panel (movie S2).
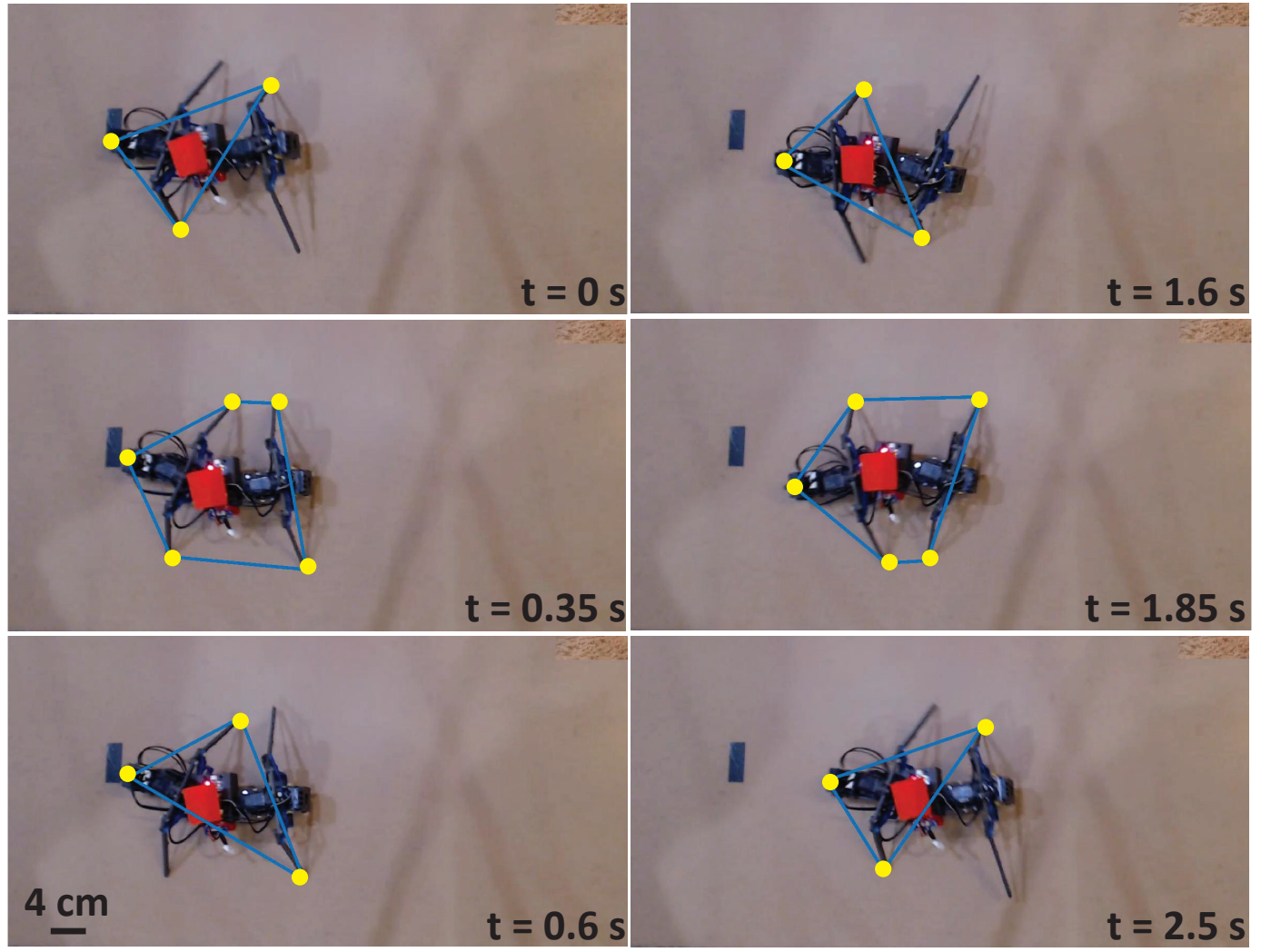
Figure S5: Stability of tail down walking. A-B The support polygon of the robot during a gait cycle (t = 2.5 s). The red marker shows the center of mass of the robot.
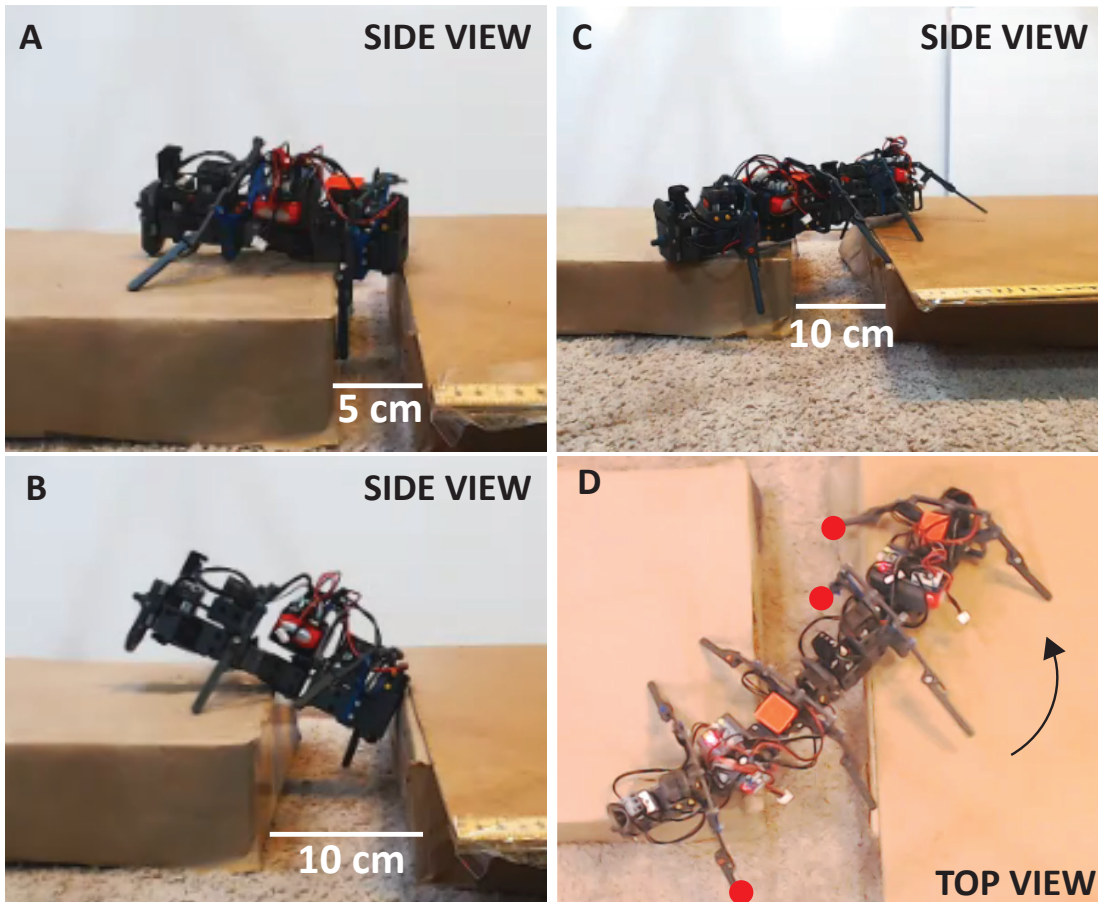
Figure S6: The most common failure modes of gap traversal experiments. A single robot attempted to traverse **A.** 5 cm and **B.** 10 cm gaps. The legs on the first segment lost the ground contact and the robot became stuck and/or the body flipped. **C-D.** Two chained robots attempted to traverse 10 cm gap. The left legs of the first two segments of the robot lost the ground contact leading to body turning (movie S3).
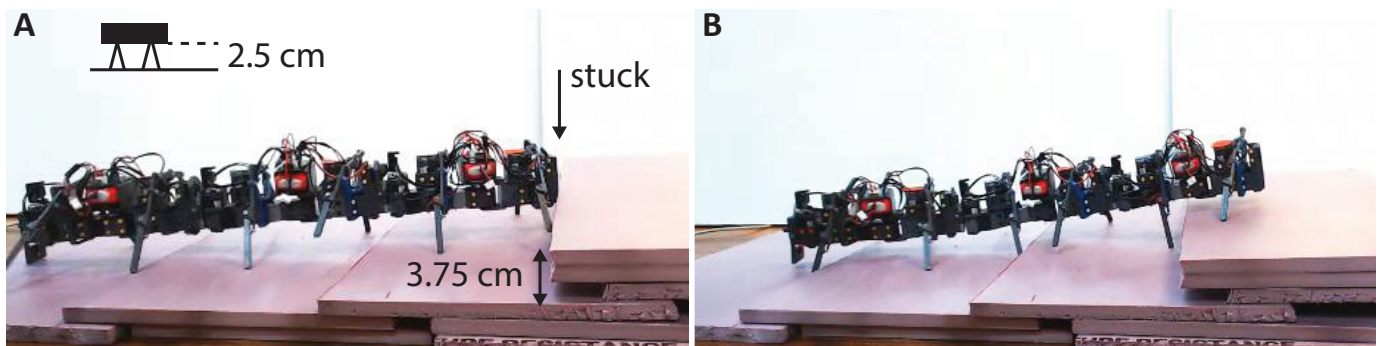
Figure S7: The failure modes of stair climbing experiments. **A.** The robot head becomes stuck if the height of the stairs (or obstacles) is 40% higher than the ground clearance of the body. **B.** When the head of a robot was manually lifted, the robot can successfully climb a stair (h = 3.75 cm, movie S3).
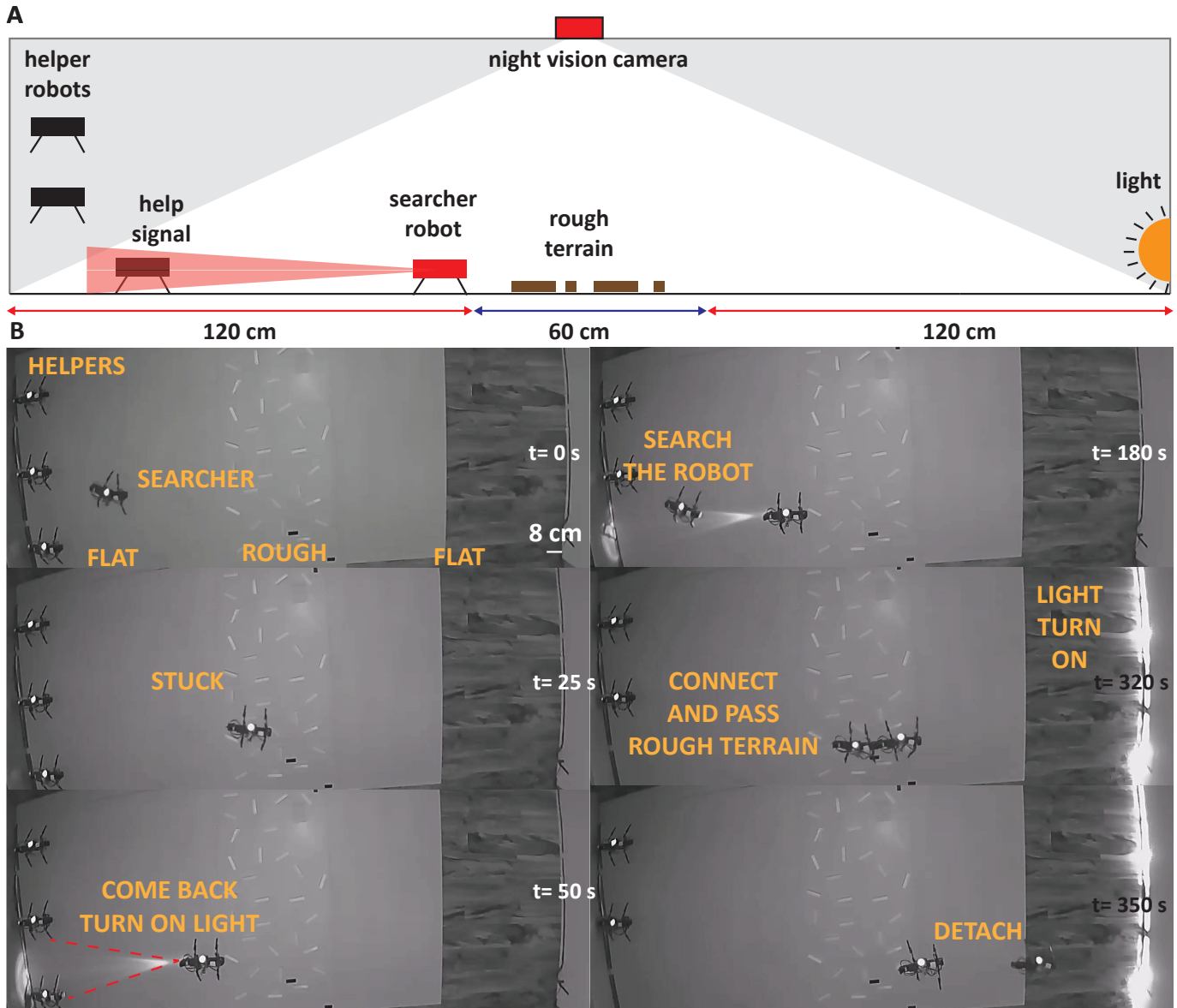
Figure S8: Autonomous swarm rough terrain traversal. A. Experimental area. A night vision camera is placed at the top of the arena and a LED light strips are attached to the end of the arena. Rectangular wooden blocks (l = 7.5, w = 1, h = 2 cm) glued onto board randomly. **B.** Helper robots stay at the beginning of the area and the searcher robot starts to walk (t = 0 s). The searcher robot becomes stuck at the obstacles (t = 25 s), comes back and turn on its aid light (t = 50 s). The robot who gets the light signal (bottom robot) searches for the stuck robot (t = 180 s) and connects to it by following the light gradient of the aid light (t = 320 s). After connection, the light source placed at the other end is tuned on. They traverse the rough terrain and disconnect at the end of the rough terrain when the front robot get close to the light (t = 350 s, movie S6).
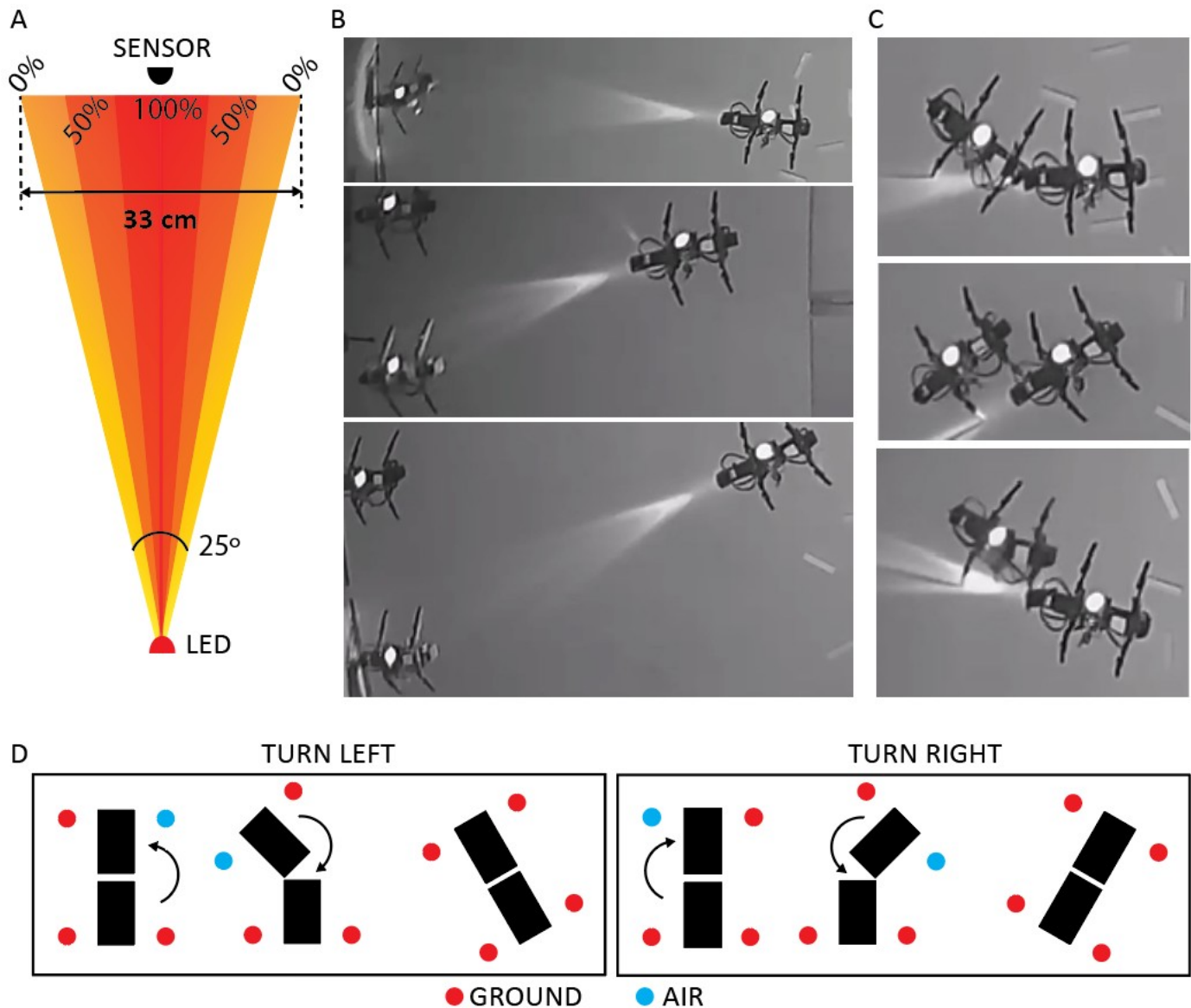
Figure S9: Robot connection statistics. A. LED light intensity range. The measured light intensity is maximum when the photo sensor sees the LED directly. **B.** Example experiments which end with a successful connection. 70% of the 20 trials successfully connected. **C.** Examples of unsuccessful connections (snapshots show the final state). The helper robot found the searcher robot, but, it could not connect due to passing the searcher robot or approaching with a sharp angle ($> 20^o$). **D.** Steps of turning gaits. To turn left/right, the robot first turns the body to the corresponding side about 45° while keeping the front leg at the side of turning on the ground. Then it rotates the body to the zero angle while keeping the opposite front leg on the ground.
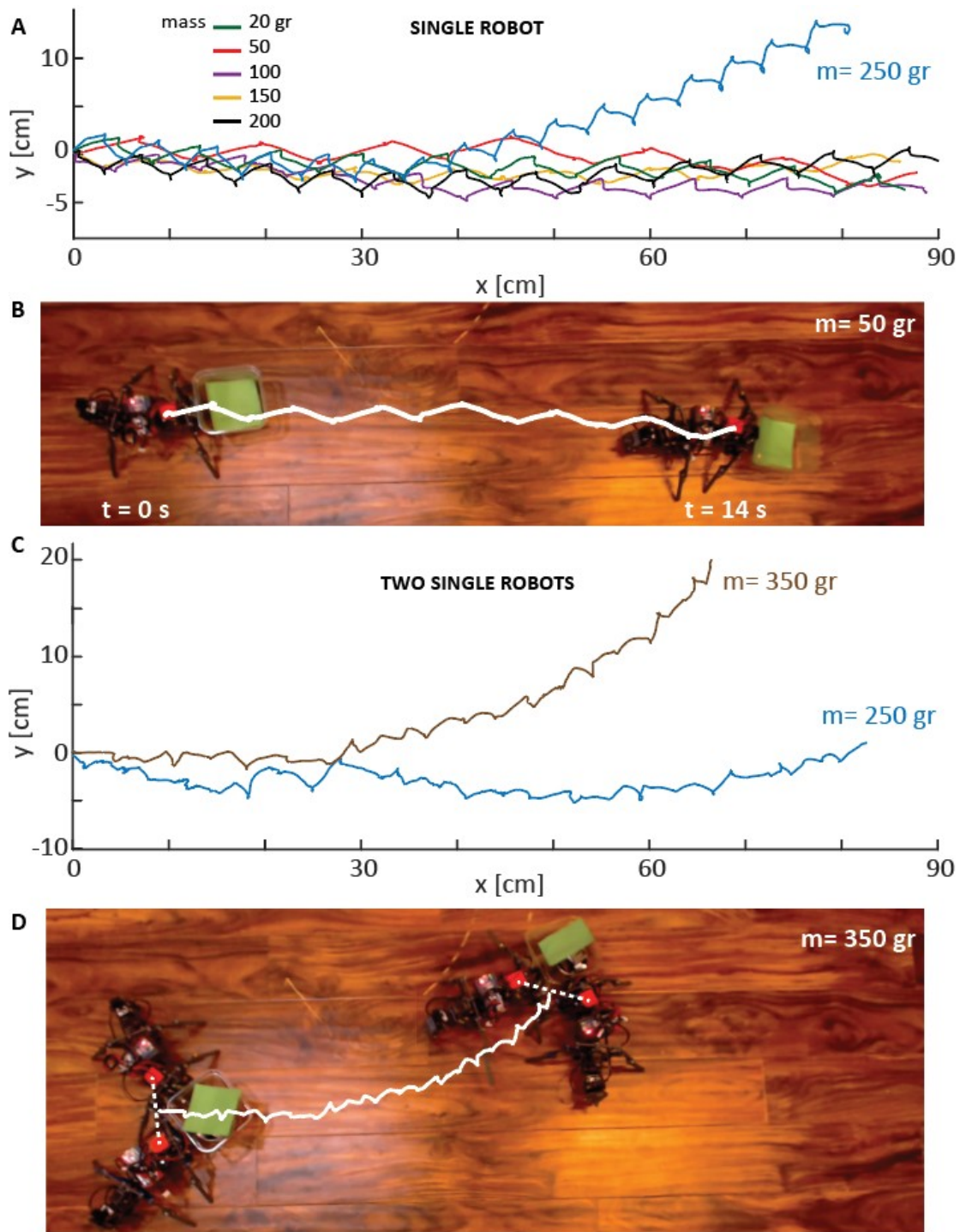
Figure S10: Single and multi robot object transport. A. Example trajectories of object transport experiments with a single robot. A rectangular box was attached to the front part of a robot. The mass of the object in the box was increased from 20 gr (green) to 250 gr (blue). **B.** Blended snapshots (at t = 0 and 14 s) from the experiment when the robot carried 50 gr object. The white trajectory shows the trajectory of the head. **C.** Example trajectories of object transport experiments with two single robots. The mass of the object in the box was increased from 250 gr (blue) to 350 gr (brown). **D.** (movie S8). Blended snapshots from the experiment when the robots carried 350 gr (blue) object. The white trajectory shows the trajectory of the center of line that connects the heads of the robots.
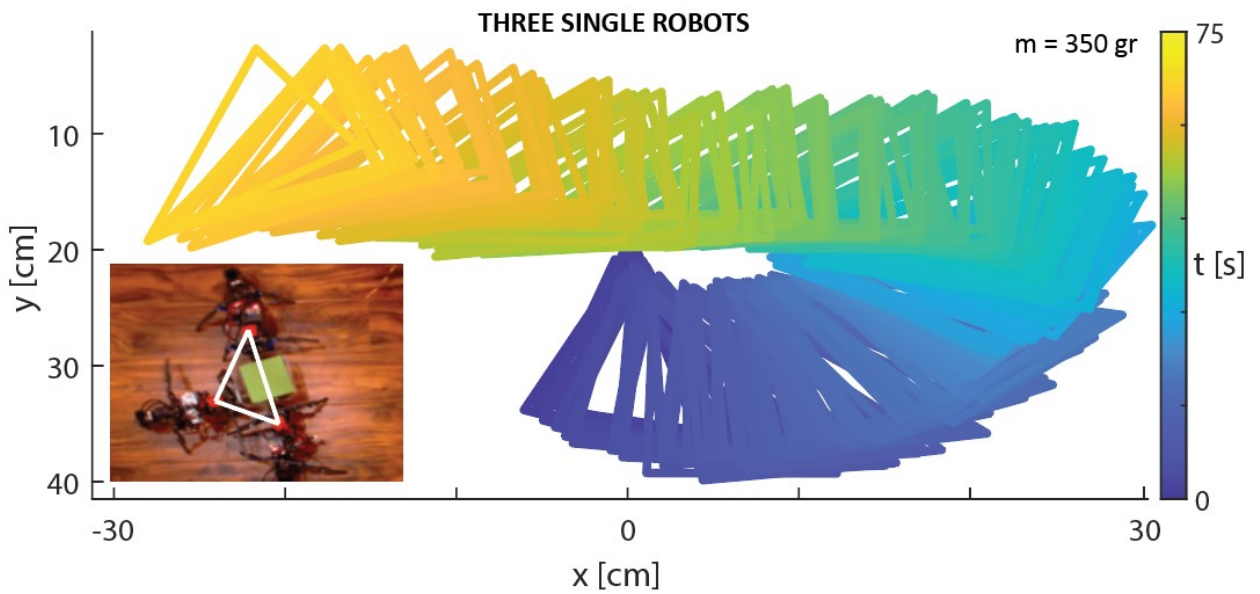
Figure S11: Object transport with three robots. A rectangular box (m = 350 gr) transported by three robots on a hardwood floor. The orientation of a white triangle that connects three robots is given as a function of time. The initial orientation of the robots are given in the inset (movie S3).
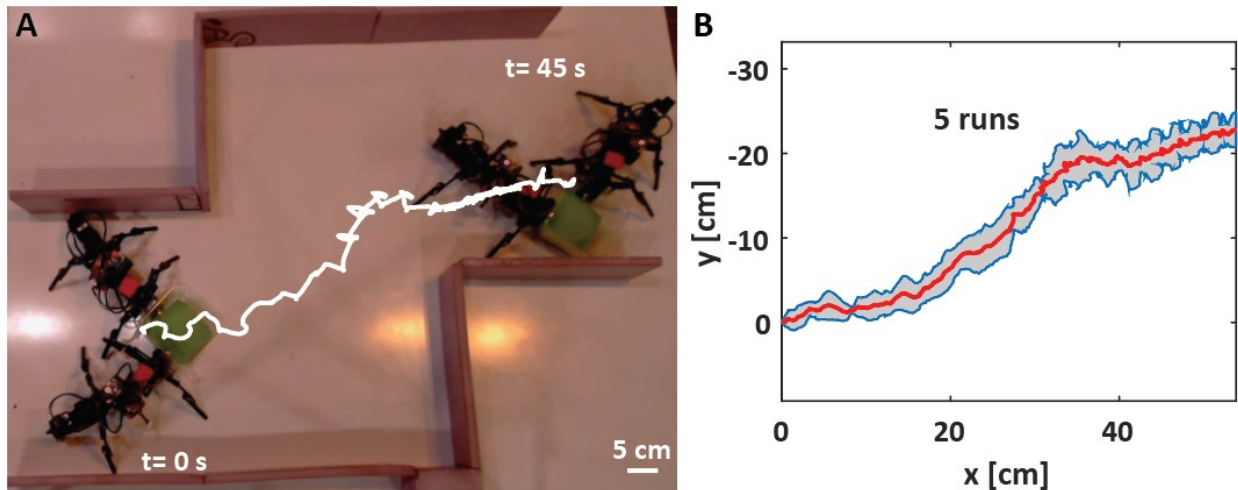

Figure S12: Object transport in a narrow tunnel. A. Two robots carry an object (m = 20 gr) in a tunnel. The white trajectory shows the trajectory of the center of the robots (the center of the line that connects the red markers on the robot) during time (0 to 45 sec.). **B.** The mean±SD (standard deviation) trajectories of 5 runs (movie S9).